RNA Therapy for Oncogenic *NRAS*-Driven Nevi Induces Apoptosis

JID Open

Dale Bryant[1,2], Sara Barberan-Martin[1,2], Ruhina Maeshima[2], Ignacio del Valle Torres[1,2], Mohammad Rabii[1,2], William Baird[2], Aimie Sauvadet[1,2], Charalambos Demetriou[2], Phoebe Jones[1,2], Nicole Knöpfel[1,2,3], Fanourios Michailidis[1,2], Melissa Riachi[1,2], Dorothy C. Bennett[4], Davide Zecchin[1,2], Alan Pittman[4], Satyamaanasa Polubothu[1,2,3], Stephen Hart[2] and Veronica A. Kinsler[1,2,3]

RAS proteins regulate cell division, differentiation, and apoptosis through multiple downstream effector pathways. Oncogenic RAS variants are the commonest drivers in cancers; however, they also drive many benign lesions predisposing to malignancy, such as melanocytic nevi, thyroid nodules, and colonic polyps. Reversal of these benign lesions could reduce cancer incidence; however, the effects of oncogenic RAS have been notoriously difficult to target with downstream pathway inhibitors. In this study, we show effective suppression of oncogenic and currently undruggable $NRAS^{Q61K}$ in primary cells from melanocytic nevi using small interfering RNA targeted to the recurrent causal variant. This results in striking reduction in expression of *ARL6IP1*, a known inhibitor of endoplasmic reticulum stress–induced apoptosis not previously linked to NRAS. We go on to show that a single dose of small interfering RNA in primary cells triggers an apoptotic cascade, in contrast to treatment with a MAPK/extracellular signal–regulated kinase kinase inhibitor. Protective packaging of the targeted small interfering RNA into lipid nanoparticles permits successful delivery into a humanized mouse model of melanocytic nevi and results in variant *NRAS* knockdown in vivo. These data show that RAS-induced protection from apoptosis is involved in persistence of *NRAS*-driven melanocytic nevi and anticipate that targeted small interfering RNA could form the basis of clinical trials for RAS-driven benign tumors.

Keywords: Melanocyte, Nanoparticle, Oncogene, siRNA, Skin

Journal of Investigative Dermatology (2025) **145,** 122–134; doi:10.1016/j.jid.2024.04.031

INTRODUCTION

The understanding of the role of oncogenic RAS proteins in human health and disease has shifted in recent years. Apart from their established role as cancer drivers, there is increasing evidence of the part they play in clonal expansion within normal tissues and in benign tumors (Dos Santos et al, 2022; Kakiuchi and Ogawa, 2021; Kakiuchi et al, 2020; Marotta et al, 2021; Martincorena et al, 2015; Nanki et al, 2020; Tang et al, 2020; van Laethem, 1999). These insights have highlighted the potential benefits of research into the early origin of RAS-driven cancers, in particular, the identification of important downstream biology that might be obscured by subsequent cancer pathogenic variants, and the tantalizing prospect of preventative therapies. Noncancer models in which oncogenic RAS can be studied and targeted therapeutically are therefore highly desirable.

The study of congenital human mosaic disorders offers exactly such an opportunity. Mosaic disorders are the result of a single-cell pathogenic variant during embryogenesis or fetal development (Kinsler et al, 2020), therefore affecting only part of the body. Over the last decade, advanced sequencing techniques comparing clinically affected with unaffected tissues have revealed the causative variants of many of these diseases. These studies have repeatedly uncovered classical oncogenic variants in *RAS* genes as the monogenic causes, with clinical diseases as distinct as arteriovenous malformations and congenital nevi resulting from the same variants affecting different embryonic cell lineages (Al-Olabi et al, 2018; Bourdeaut et al, 2010; Groesser et al, 2012; Kinsler et al, 2013b). In retrospect, their role in these diseases makes perfect sense: these variants govern cell proliferation, differentiation, and apoptosis, which are the underlying mechanisms of embryogenesis as much as they are of cancer. It also makes sense of the clinical phenotypes because many of these mosaic diseases are known to have a cancer predisposition (Bourdeaut et al, 2010; Hafner et al, 2011; Kinsler et al, 2017a). Because the variants are usually incompatible with life in the germline, they generally result in sporadic disease, a disease mechanism predicted decades before the variants were found (Happle, 1987).

Congenital melanocytic nevus (CMN) syndrome is a mosaic neurocutaneous disease. The phenotype includes skin

[1]*Mosaicism and Precision Medicine Laboratory, The Francis Crick Institute, London, United Kingdom;* [2]*Genetics and Genomic Medicine, UCL Great Ormond Street Institute of Child Health, London, United Kingdom;* [3]*Paediatric Dermatology, Great Ormond Street Hospital for Children, London, United Kingdom; and* [4]*St George's University of London, London, United Kingdom*

Correspondence: Veronica A. Kinsler, Mosaicism and Precision Medicine Laboratory, The Francis Crick Institute, 1 Midland Rd, London NW1 1AT, United Kingdom. E-mail: v.kinsler@ucl.ac.uk

Abbreviations: CMN, congenital melanocytic nevus; ER, endoplasmic reticulum; MEKi, MAPK/extracellular signal–regulated kinase kinase inhibitor; RNAseq, RNA sequencing; RTNP, receptor-targeted nanoparticle; siRNA, small interfering RNA; WT, wild-type

Received 10 November 2023; revised 4 April 2024; accepted 16 April 2024; accepted manuscript published online 17 June 2024; corrected proof published online 12 August 2024

lesions from birth that are most easily understood by analogy to acquired melanocytic nevi. However, because CMNs arise in prenatal rather than postnatal life, they differ from acquired melanocytic nevi in their size, being capable of covering up to 80% of the skin surface (graphical abstract). In acquired melanocytic nevi, the single-cell pathogenic variant likely affects a specified melanocyte, producing a single nevus. In CMN, the pathogenic variant affects a melanocytic precursor at some point in its developmental trajectory and can therefore produce a very broad phenotypic spectrum. This ranges from multiple cutaneous nevi with associated multisystem abnormalities (earlier event) to a small single nevus (later event). The more severe multiple CMN phenotypes are therefore rarer than the small single nevi, resulting in a continuum of incidence at birth ranging from approximately 1 in 20,000 (Castilla et al, 1981) to 1 in 100 (Alper and Holmes, 1983; Jacobs and Walton, 1976), respectively.

Severe CMN phenotypes are a major source of morbidity and are associated with an increased mortality in childhood. They cause intractable itch, recurrent infections, recurrent development of nodules requiring assessment for malignancy, and difficulties with psychological adjustment in individuals and their families (Masnari et al, 2019). When melanoma arises in childhood, it is generally rapidly fatal (Kinsler et al., 2017a). Patients are much in need of an effective treatment for their congenital disease, and the promise of such a treatment would bring with it the prevention of melanoma development as well as providing proof of concept for RAS-driven benign tumor reversal.

CMN is caused in 67% of cases by recurrent oncogenic variants in gene *NRAS*, and the *NRAS* c.181C>A, p.(Q61K) variant is the commonest cause across the whole phenotypic spectrum (Kinsler et al, 2013b; Polubothu et al, 2020). Because of the understanding of the genetic causes (Barberan Martin, 2023; Etchevers et al, 2018; Kinsler et al, 2013b; Martins da Silva et al, 2019; Polubothu et al, 2020; Salgado et al, 2015), pathway-targeted cancer therapies have been repurposed as potential treatments for CMN, although oncogenic *RAS* variants are notoriously difficult to target with small molecules (Molina-Arcas et al, 2021). The first used was oral MAPK/extracellular signal–regulated kinase kinase inhibitor (MEKi) trametinib for CMN-associated leptomeningeal melanoma, for which there was some benefit in alleviating symptoms before eventual relapse in a case series (Kinsler et al, 2017b; Küsters-Vandevelde et al, 2014), but the CMNs themselves remain stubbornly unchanged. Since then, trametinib has also been used successfully to reduce postnatal expansion of nodules in *BRAF*-fusion CMN (Martin et al, 2024; Mir et al, 2019); however, again, the underlying disease phenotype is unaffected.

These facts led us to conclude that although MAPK activation is involved in postnatal proliferations (proliferative nodules and melanoma) and may be important during in utero development, the life-long persistence of CMN in the skin is likely not driven by the MAPK pathway. We reasoned that targeting the root cause of the disease, the pathogenic variant itself, would be the best precision medicine approach and may reveal the downstream pathways of disease persistence. We therefore set out to design targeted genetic therapy for CMN, with a view to testing this in laboratory models. Silencing RNAs targeted specifically at the variant allele were developed and then incorporated into receptor-targeted lipid nanoparticles designed to home preferentially to nevus cells. Targeted silencing was demonstrated in primary patient nevus cells in vitro, and in a humanized transgenic mouse in vivo. Importantly, silencing of the variant allele triggered apoptosis of nevus cells in vitro through a previously unsuspected link to the endoplasmic reticulum (ER) stress–induced apoptosis pathway.

These findings highlight the power of studying oncogenic RAS variants in benign diseases to identify downstream biological pathways and demonstrate proof of concept that such lesions may be reversible. As such, this therapeutic approach paves the way not only for potential CMN resolution in humans but as a potential paradigm for preventative cancer therapies in benign tumors driven by oncogenic RAS.

RESULTS

Design and optimization of small interfering RNA in HCT116 cells

Variant NRAS c.181C>A transcript expression can be selectively silenced in HCT116 cells. RT-qPCR primers specific to the $NRAS^{c.181C>A}$ variant and wild-type (WT) alleles were designed (Supplementary Table S1), and specificity was confirmed in homozygous $NRAS^{c.181C>A}$ HCT116 colorectal carcinoma cell line C6072C (CrownBio) with matched parental WT C8052C-WT line (CrownBio). Nineteen 21mer small interfering RNAs (siRNAs) were designed by a walked approach spanning the variant of interest (Figure 1a). RT-qPCR screening of this panel in the paired HCT116 lines identified 3 siRNAs (siRNAs 8, 14, and 15), which significantly reduced expression of variant ($NRAS^{Q61K}$; $P \leq .05$) compared with that of the WT transcripts ($NRAS^{WT}$; $P > .05$) (Figure 1b). Allelic discrimination was further assessed using 2 published formulae (Takahashi and Hohjoh, 2014) (Figure 1c). Both identified 5 siRNAs as likely candidates (siRNA8, 10, 12, 13, and 15), all positioning the missense variant within a central window of the siRNA (Figure 1c), which was consistent with previous data on siRNA single-base targeting (Takahashi and Hohjoh, 2014). siRNAs 8 and 15 were therefore selected for further study, in addition to siRNA1, as an effective silencer of expression of both alleles and therefore a useful control. All 3 of the selected candidates reduced MAPK pathway activation in $NRAS^{c.181C>A}$ mutant HCT116 (Supplementary Figure S1a).

siRNA8 has fewest off-target effects on RNA-sequencing in HCT116 cells. Transcriptome-wide RNA sequencing (RNAseq) was undertaken on paired C6072C and C8052C-WT cells with and without treatment with siRNAs 1, 8, and 15 to identify and quantify both on- and off-target effects. Baseline *NRAS* expression levels were lower in the C6072C homozygous variant line (Figure 1d) than in the C8052C-WT parent line (Figure 1e) for unknown reasons. Variant *NRAS* expression by RNAseq analysis in C6972C cells was silenced to 9, 79, and 64% of untreated levels by siRNAs 1, 8, and 15, respectively (Figure 1d). Variant allele specificity was confirmed for siRNAs 8 and 15 but not for siRNA1 as previously demonstrated (Figure 1d and e). In contrast to the qPCR data, there was also a small but statistically significant

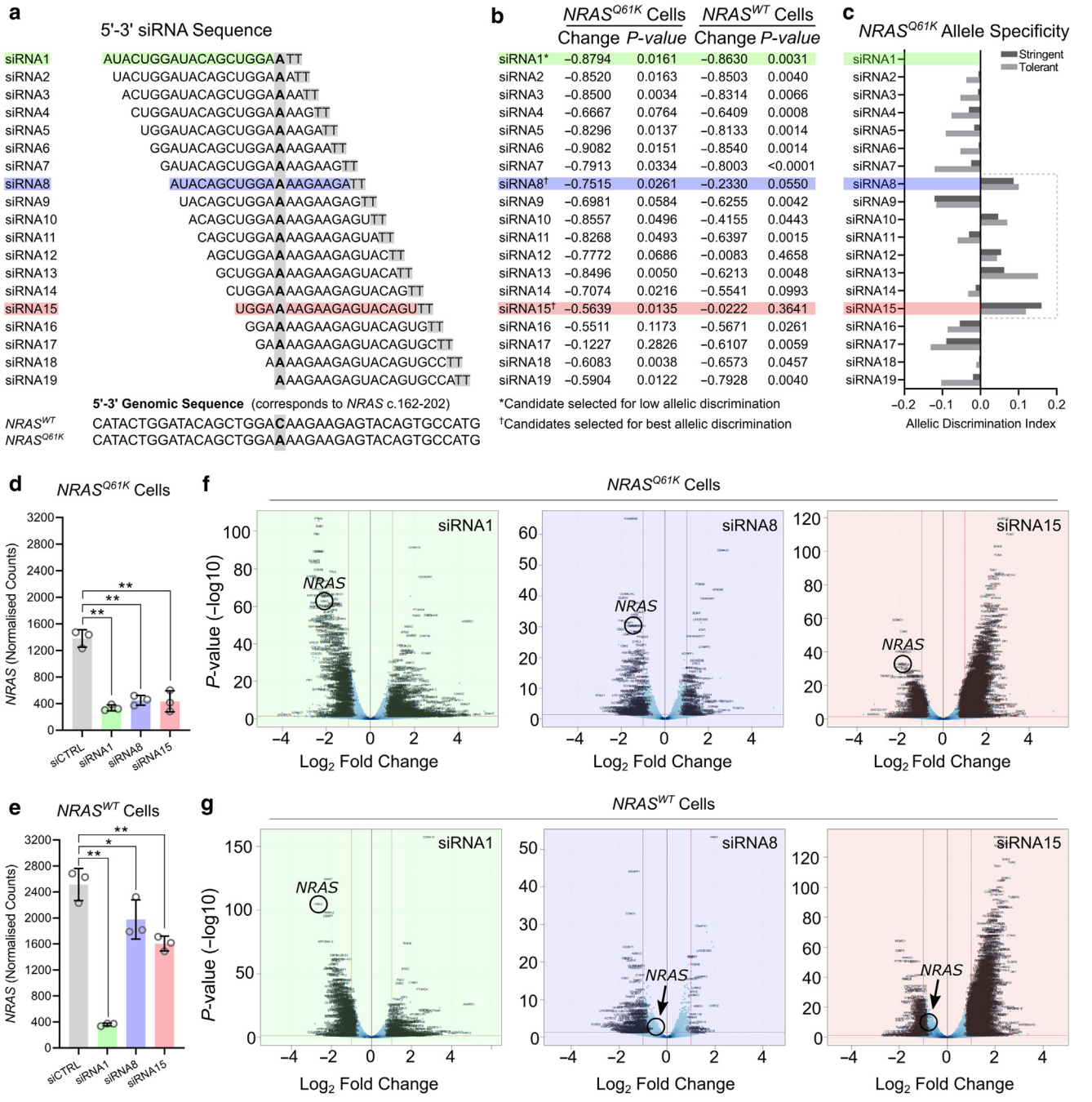

Figure 1. Identification of siRNA with allelic discrimination for nevus cell causing *NRAS* variant. **(a)** siRNAs were designed with a walking approach over the variant of interest (*NRAS* c.181C>A; p.Q61K) (vertical gray bar). Note that the sequences illustrated in the panel are the passenger strands for ease of interpreting corresponding nucleotides. siRNAs 1, 8, and 15 are color coded for reference in other panels of this figure. **(b)** The impact of siRNA treatment (48 hours) on *NRAS* transcript expression was investigated in HCT116 cells with qPCR. siRNA8 (blue) and siRNA15 (red) were selected on the basis of their propensity to reduce expression of the *NRAS* variant and not WT *NRAS*. siRNA1 (green) was included in these experiments as a comparative control because it minimized both variant and WT *NRAS* expressions. **(c)** Assessment of allelic discrimination. Positive values indicate specificity for the *NRAS* variant; negative values indicate specificity for the *NRAS* WT mRNA transcript. **(d, e)** RNAseq confirms that the selected candidates do selectively minimize expression of the **(d)** *NRAS* variant compared with **(e)** WT *NRAS*. **(f, g)** Volcano plots demonstrating the impact of siRNA candidates on the transcriptome. Circles/arrows mark the position of *NRAS* in this dataset. n = 3 replicates; bars = mean; error bars = SD, with 1-way ANOVA. RNAseq, RNA sequencing; siRNA, small interfering RNA; WT, wild-type.

reduction of the *NRAS* WT transcript seen with siRNAs 8 and 15 (Figure 1e). siRNA8 alone did not affect the expression of *NRAS* homologs *KRAS* and *HRAS* in nonvariant cells (Supplementary Figure S1b and c). Expression of genes containing sequences similar to the target sequence of each siRNA was assessed, revealing that siRNA8 had fewer off-target effects than siRNA15 (Supplementary Figure S1d–f). Pathway analysis of all 2-fold ($P \leq .05$) differentially expressed genes was performed using Metascape (Zhou et al, 2019). siRNA8 had the most limited impact on the

transcriptome while maintaining allele specificity and fewest off-target effects (Figure 1f and g and Supplementary Data S1).

On this basis, siRNA8 was selected as the lead candidate siRNA—henceforth termed si$NRAS^{Q61K}$. Testing of si$NRAS^{Q61K}$ then moved from the cancer cell line to primary patient cells. Although this removes the possibility of a control population—there are no genetically normal nevus cells—we consider it to be a much more physiological in vitro model: first, the cells are heterozygous for the $NRAS^{Q61K}$ variant; second, the cell type is the target of therapy; and finally, this model introduces physiological intersample germline that which will be the reality in clinical trials.

siRNA knockdown in primary CMN cell cultures

si$NRAS^{Q61K}$ selectively knocks down the expression of the variant transcript in primary CMN cell cultures. Eight pure primary CMN cell cultures were established (Figure 2a and Supplementary Figure S2a–d), and the heterozygous causal variant was confirmed by Sanger sequencing after expansion (Figure 2b). Nevus cells (n = 4) were treated with a single dose of si$NRAS^{Q61K}$, and results were analyzed at 48 hours. Treatment suppressed the *NRAS* variant allele mRNA levels significantly more than the WT (Figure 2c–e and Supplementary Figure S2e). In the absence of an $NRAS^{Q61K}$-specific antibody, total NRAS protein (combined $NRAS^{WT}$ and $NRAS^{Q61K}$) was demonstrated to be significantly reduced (Figure 2f and g and Supplementary Figure S2g).

si$NRAS^{Q61K}$ does not alter classical melanocytic markers on primary CMN cell cultures. Baseline characterization of nevus cells to confirm melanocytic lineage characterized SOX10 and tyrosinase expression by immunocytochemistry, in addition to MITF, DCT, and Nestin (Supplementary Figure S3a–e) and markers of senescence p53 (*TP53*) and p16 (*CDKN2A*) (Supplementary Figure S3f and g). Despite an increase in *DCT* expression and a small decrease in *NES* expression seen in the RNAseq dataset (Supplementary Figure S3d and e), all immunocytochemical markers were unaffected by si$NRAS^{Q61K}$ treatment at 48 hours (Supplementary Figure S3a–g).

si$NRAS^{Q61K}$ reduces MAPK pathway activation and proliferation rate in primary CMN cell cultures. Primary cells from 4 patients with $NRAS^{Q61K}$ CMN were treated with a single dose of si$NRAS^{Q61K}$, after which immunoblotting demonstrated significantly decreased levels of phosphorylated extracellular signal–regulated kinase/extracellular signal–regulated kinase ratio at 48 hours (Figure 2f and h and Supplementary Figure S2g). Cells were monitored with 5-ethynyl-2′-deoxyuridine incorporation (Figure 2i) and live-cell imaging (Figure 2j) from 24 to 48 hours after treatment, revealing reduction in proliferation compared with that of nontargeting siRNA controls (Figure 2i and j), an effect that was dose dependent (Supplementary Figure S2f).

si$NRAS^{Q61K}$ reduces the proportion of nonpolar cells in primary nevus cell cultures. Label-free ptychographic imaging of nevus cell morphology and behavior in samples from 4 patients demonstrated a range of morphologies within each sample (Supplementary Figure S2b and c). Morphologies were therefore classified using a machine learning tool into relative proportions of nonpolar, bipolar, multipolar, and large multinucleated likely senescent cells (Supplementary Figure S4a and b and Supplementary Figure S5). The fractions of each cell type were consistent between patients (Supplementary Figure S4d). The nonpolar morphology generally appeared briefly before a cell division (Supplementary Figure S4e), which was notable sometimes in 3 daughter cells (Supplementary Figure S4g and Supplementary Video S1). A single dose of si$NRAS^{Q61K}$ treatment induced a significant decrease in the fraction of nonpolar cells with no other subtype alterations at 48 hours (Supplementary Figure S4c). Flow cytometry based on DNA content (DAPI intensity) analysis did not detect an impact on cell cycle stages after 48 hours of si$NRAS^{Q61K}$ treatment (Supplementary Figure S2k).

si$NRAS^{Q61K}$ treatment of primary CMN cells suppresses anti-apoptotic marker ARL6IP1. RNAseq was performed on primary nevus cell lines before and after treatment with si$NRAS^{Q61K}$ to look for both on- and off-target effects. Expression of variant *NRAS* was significantly and preferentially downregulated compared with that of WT (Figure 2e), whereas highly homologous genes *KRAS* (Supplementary Figure S2h) and *HRAS* (Supplementary Figure S2i) were unaffected. Pathway analysis of differentially expressed genes identified enrichment primarily for pathways associated with the cell cycle (Figure 2k and Supplementary Figure 2j and Supplementary Data S2). The RAL and integrin pathways were also enriched along with pathways associated with neuronal ensheathment (Figure 2k and Supplementary Figure S2j and Supplementary Data S2). In contrast, genes associated with melanocyte differentiation were largely unaffected, except for an increase in the expression of *DCT* (Figure 2k and Supplementary Figure S3e). Importantly, the most significantly differentially expressed gene was *ARL6IP1*, also known as *ARMER* (apoptosis regulator in the ER membrane) (Figure 2l).

si$NRAS^{Q61K}$ treatment triggers apoptosis in primary CMN cell cultures. As highlighted earlier, *ARL6IP1* is highly expressed in nevus cells (Supplementary Figure S3h), with a distribution across the ER membrane in a pattern similar but not identical to the rough ER associated protein RPN1 (Figure 3a). Validation experiments demonstrated that 48 hours of si$NRAS^{Q61K}$ treatment results in suppression of *ARL6IP1* gene (Figure 3b) and protein (Figure 3c and Supplementary Figure S3i) in all patient lines. *ARL6IP1* was also significantly downregulated in the HCT116 cells treated with si$NRAS^{Q61K}$ dataset (Supplementary Figure S6a and b). *ARL6IP1* is known to have a role in protecting cells from the apoptotic effects of ER stress (Lui et al, 2003), and oncogenic NRAS activity has been demonstrated to drive resistance to ER stress (Bright et al, 2018). We therefore reviewed the expression of key ER stress–induced apoptosis regulators *ERN1*, *EIF2AK3* (*PERK*), *ATF6*, *ATF4*, and *GRP78* (Supplementary Figure S6). *ERN1* and *EIF2AK3* (*PERK*) were significantly increased on RNAseq (Supplementary Figure S6d–f), but only *ERN1* was found to be significantly upregulated in response to si$NRAS^{Q61K}$ treatment

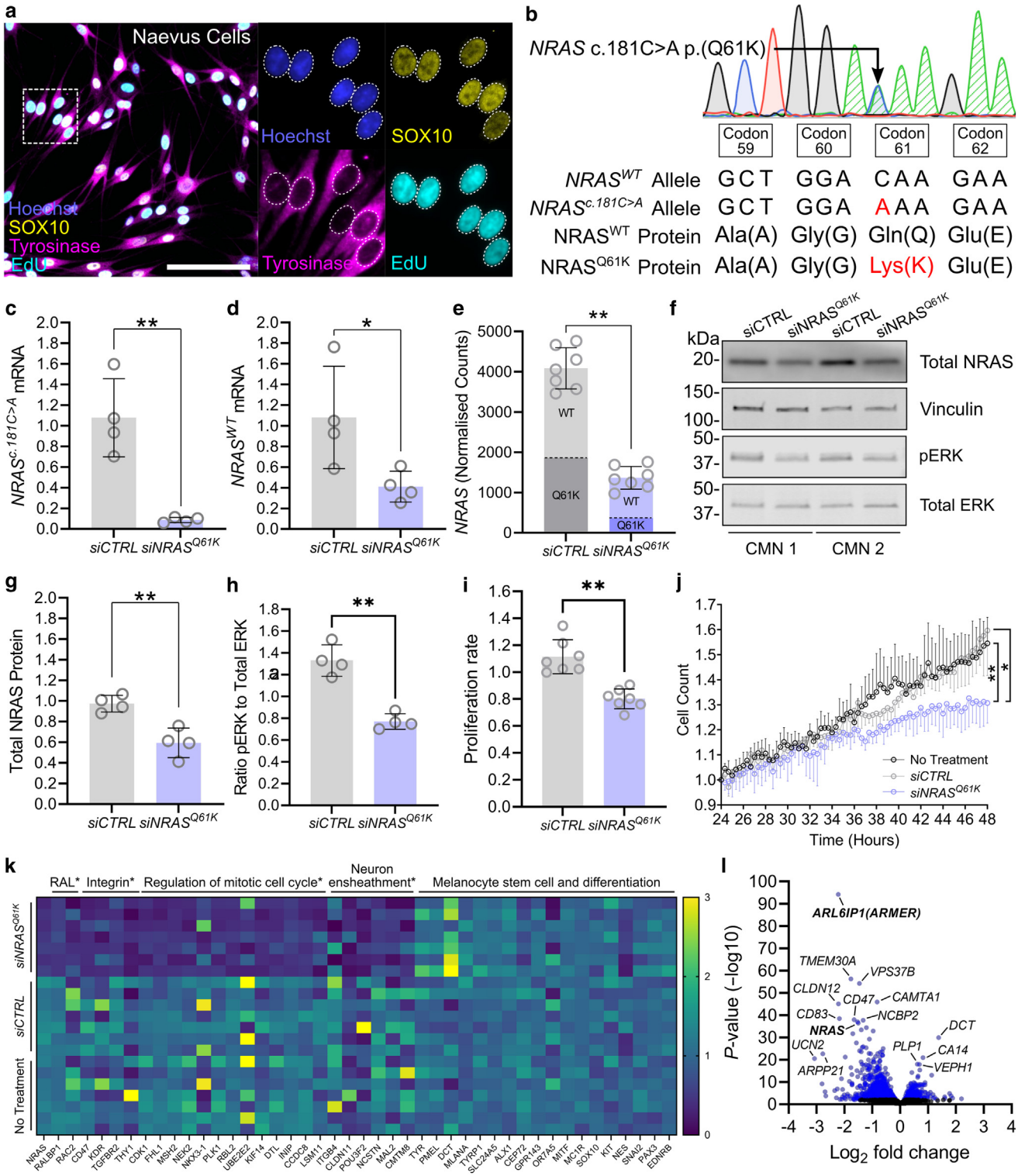

Figure 2. si*NRAS*^{Q61K} treatment decreases MAPK activation and reveals pathways/genes regulated by *NRAS*^{Q61K} expression in nevus cells. (**a**) In vitro culture of patient-derived nevus cells without feeder cells. Nevus cells are positive for nuclear melanocyte marker SOX10 and cytoplasmic melanocyte marker tyrosinase. Bar = 100 μm. (**b**) Selective proliferation of patient-derived nevus cells reveals the somatic *NRAS* c.181C>A variant. (**c**) Relative levels of *NRAS*^{Q61K} (*NRAS*$^{c.181C>A}$) mRNA after si*NRAS*^{Q61K} treatment normalized to those of untreated cells. (**d**) Relative levels of *NRAS*^{WT} mRNA after si*NRAS*^{Q61K} treatment normalized to those of untreated cells. (**e**) RNAseq normalized counts for *NRAS*. Fraction of *NRAS*^{WT} and *NRAS*^{Q61K} transcript were calculated on the basis of reads covering the location of the *NRAS* variant. (**f**–**h**) Relative levels of total (**f, g**) NRAS protein and (**f, h**) MAPK activation (pERK) after si*NRAS*^{Q61K} treatment normalized to those of untreated cells. (**i**) Relative proliferation rate as assessed with EdU incorporation during final 24 hours of si*NRAS*^{Q61K} treatment (48 hours). (**j**) Relative proliferation of nevus cells during 48-hour treatment (24–48 hours) using ptychographic imaging/analysis. (**k**) Heatmap illustrating genes in pathways responding to si*NRAS*^{Q61K} (*Metascape WP2290 RALA downstream regulated genes; M53 PID INTEGRIN3 PATHWAY; GO:0007346 regulation of mitotic cell cycle; GO:0007272 ensheathment of neurons; GO:0008366 axon ensheathment) and melanocyte stem cell and differentiation associated genes, which were relatively unaffected. (**l**) Volcano plot illustrating fold change and false discovery rate. Genes with very strong significance and fold change are

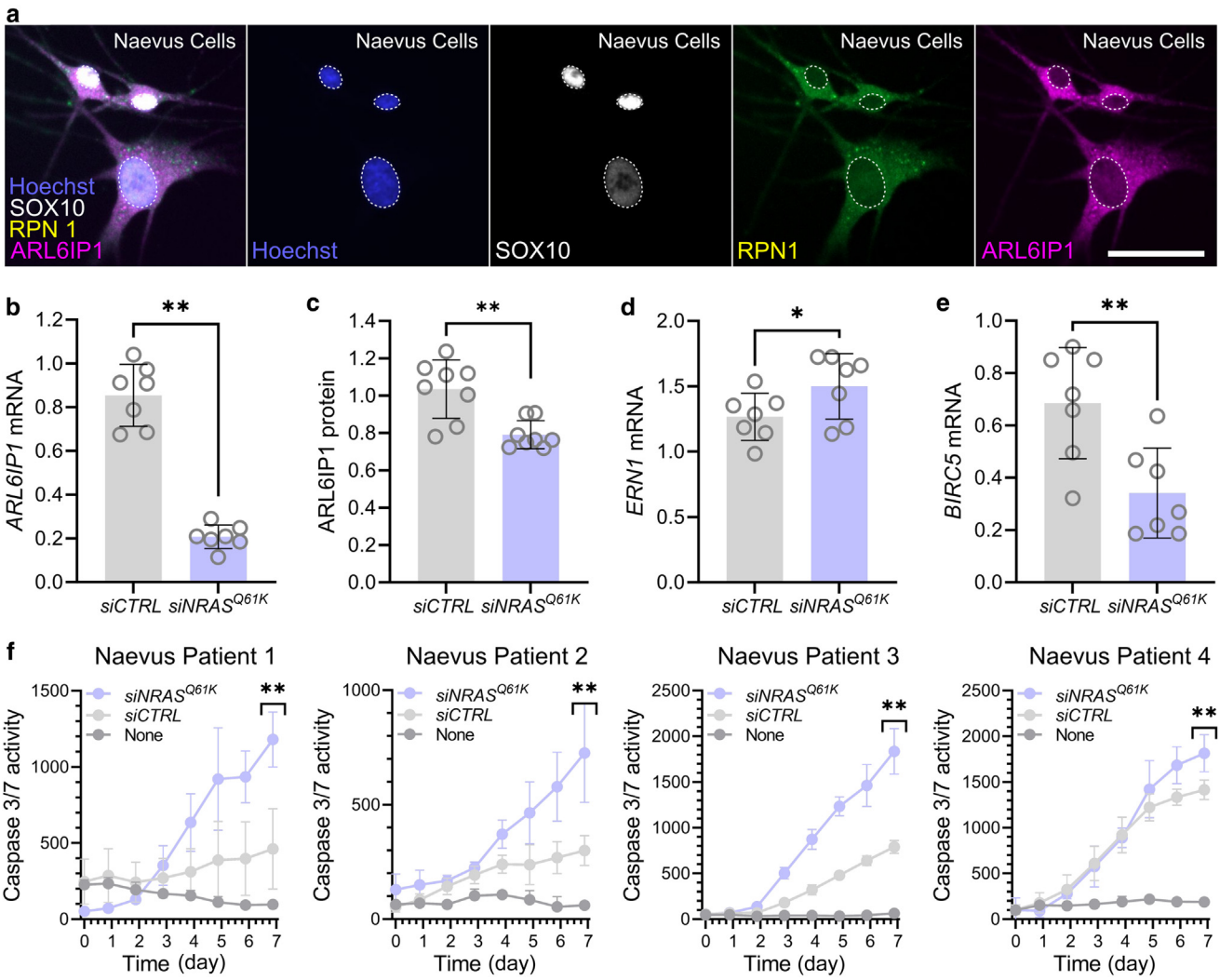

Figure 3. Treatment of nevus cells with si*NRAS*^{Q61K} leads to ER stress and apoptosis. (**a**) ER-localized expression of ARL6IP1 in patient-derived nevus cells. Bar = 50 μm. (**b**–**e**) After 48 hours of treatment with si*NRAS*^{Q61K}, (**b**) the expression of *ARL6IP1* mRNA is decreased, (**c**) the expression of ARL6IP1 protein is decreased, (**d**) the expression of ER stress sensor *ERN1 (IRE1)* is increased, and (**e**) the expression of antiapoptotic survivin (*BIRC5)* is decreased. (**f**) Caspase 3/7 activity in cells treated with si*NRAS*^{Q61K} over 7 days. n = 7 patients (for **b**, **d**, and **e**) and n = 8 patients (for **c**). Bars = mean, and error bars = SD, with 1-tailed unpaired *t*-test. n = 4, bars = mean, and error bars = SD, with 2-way ANOVA (for **f**). ER, endoplasmic reticulum; siCTRL, control-targeted small interfering RNA.

at 48 hours with qPCR (Figure 3d and Supplementary Figure S6g). In parallel, we identified a significant reduction *BIRC5* expression with si*NRAS*^{Q61K} treatment in both the nevus cells (Figure 3e) and the HCT116 cell datasets (Supplementary Figure S6c). *BIRC5* encodes survivin, a key protein in protection of RAS-inducted apoptosis.

Given these early indicators of activation of apoptosis pathways on RNAseq at 48 hours, we then measured apoptosis using caspase 3/7 activation in live imaging of cells from 4 patients with nevus over a period of 7 days. All nevus cell cultures treated with a single dose of si*NRAS*^{Q61K} showed markedly increased levels over that period in all patients compared with untreated cells and control siRNA by 7 days, emerging from around 3–4 days (Figure 3f).

siNRAS*^{Q61K} *treatment in primary nevus cell cultures permits effectiveness of MEKi. The effectiveness of si*NRAS*^{Q61K} treatment was then compared with that of MEKi trametinib—currently, the only medical therapy to have been tried in patients with CMN in vivo. Very few proliferating nevus cells were detected when treated with 5 nM trametinib, and almost no proliferating cells were detected when treated with 12.5 nM trametinib (Figure 4a and b). The effectiveness of si*NRASQ61K* on reducing proliferation was not detected at these concentrations (Figure 4a and b). The effects of combining trametinib and siNRASQ61K on caspase 3/7 activity were monitored over 5 days because the previous experiment (Figure 3f) revealed an effect by that time point. Unlike its effects on proliferation of CMN cells in culture,

labeled. n = 4 patients (for **c**, **d**, **g**, and **h**) and n = 7 patients (for **e, i, k,** and **l**). Bars = mean; error bars = SD, with 1-tailed unpaired *t*-test. n = 4 patients; points = mean; error bars = SD, with 1-way ANOVA (for **j**). CMN, congenital melanocytic nevus; EdU, 5-ethynyl-2′-deoxyuridine; ERK, extracellular signal–regulated kinase; GO, Gene Ontology; pERK, phosphorylated extracellular signal–regulated kinase; RNAseq, RNA sequencing; siCTRL, control-targeted small interfering RNA.

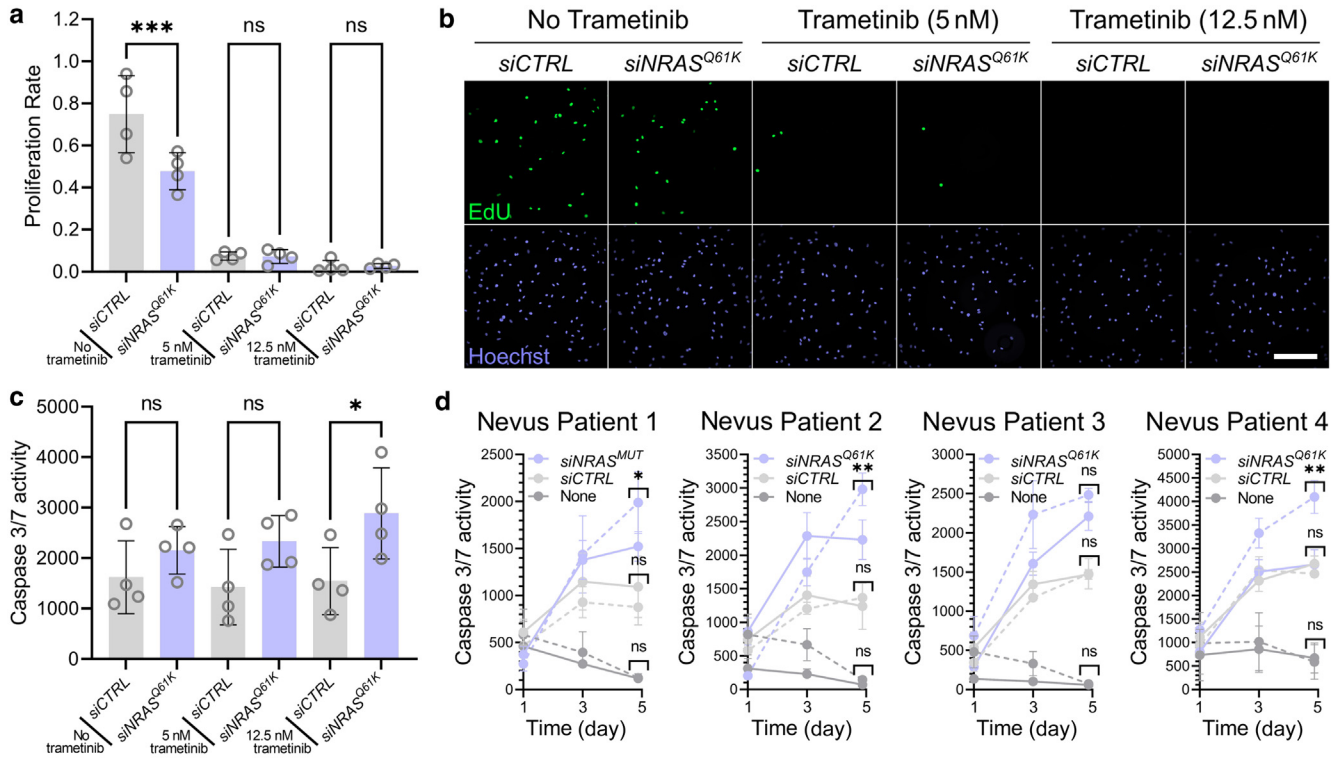

Figure 4. Treatment of nevus cells with si*NRAS*^{Q61K} permits effectiveness and synergy with trametinib. (**a, b**) Relative proliferation rate as assessed with EdU incorporation during final 24 hours of combined si*NRAS*^{Q61K} and trametinib treatment (5 nM and 12.5 nM) (48 hours). Bar = 200 μm. (**c**) Caspase 3/7 activity in patient nevus cells after 5 days of treatment with si*NRAS*^{Q61K} in combination with trametinib (5 nM and 12.5 nM). (**d**) Caspase 3/7 activity in cells treated with (perforated line) or without (solid line) 12.5 nM trametinib in combination with si*NRAS*^{Q61K} over 5 days. n = 4 patients. Bars = mean, and error bars = SD, with 1-way ANOVA (for **a** and **c**). n = 5 technical replicates for each patient, points = mean, and error bars = SD, with 1-way ANOVA (for **d**). EdU, 5-ethynyl-2′-deoxyuridine; siCTRL, control-targeted small interfering RNA.

MEKi trametinib alone had no impact on caspase 3/7 activity (Figure 4c and d). However, addition of 12.5 nM trametinib to si*NRAS*^{Q61K}-treated cells significantly increased the induction of apoptosis seen with si*NRAS*^{Q61K} treatment alone, an effect not seen with addition of trametinib to siRNA-targeted control—treated cells (Figure 4c and d).

Design and testing of receptor-targeted nanoparticles

Designing a delivery system for siRNA treatment was done with extrapolation to human trials in mind. Although we had already incorporated allele targeting within the siRNA design, additional targeting of the cell type was considered desirable to keep the eventual required dose as low as possible. The KIT receptor was selected as the most melanocyte-specific cell surface target compared with that of other skin cells on the basis of single-cell expression data (Uhlén et al, 2015) and because a peptide sequence for targeting had already been established in a previous publication (Reshetnyak et al, 2013).

Optimization of self-assembling receptor-targeted nanoparticles protects siRNA from degradation and allow delivery into human skin explants. Self-assembling receptor-targeted nanoparticles (RTNPs) have previously been described as highly effective methods of intracellular delivery for siRNA (Tagalakis et al, 2014). Formulation of the RTNPs was optimized using variable peptide content, while maintaining equal mass ratios of siRNA and lipid (Supplementary Figure S7a—c), producing si*NRAS*^{Q61K} RTNPs. Mean nanoparticle diameter was assessed using dynamic light scattering at approximately 200 nm (Supplementary Figure S7a and f). Addition of increasing amounts of peptide altered the lipid nanoparticles from anionic to cationic (Supplementary Figure S7b) and, in parallel, resulted in increased siRNA encapsulation. Encapsulation was complete at ratios 1:3:1 and 1:4:1 (lipid:peptide:siRNA) (Supplementary Figure S7c) and protected the siRNA from RNase degradation (Supplementary Figure S7d). Treatment of nevus cells with RTNPs containing a peptide sequence reported to bind to the KIT receptor delivered siRNA to the cells (Supplementary Figure S7g). si*NRAS*^{Q61K} RTNPs were successfully delivered to the dermis of skin explants of patients with CMN after intradermal injection (Figure 5a and b).

Treatment with *siNRAS*^{Q61K} RTNPs in a murine model of CMN

Cy5-siRNA in RTNPs can be delivered successfully into mouse dermis. To demonstrate in vivo delivery, Cy5-tagged control siRNA incorporated into RTNPs was injected into mouse dermis, and skin was fixed 1 hour later. Fluorescence was visualized after paraffin embedding and H&E staining, confirming successful delivery into the dermis (Supplementary Figure S8c and d).

Treatment with siNRAS*^{Q61K} *RTNPs induces selective knockdown of variant humanized NRAS. Treatment with si*NRAS*^{Q61K} RTNPs was then tested in a murine model of CMN

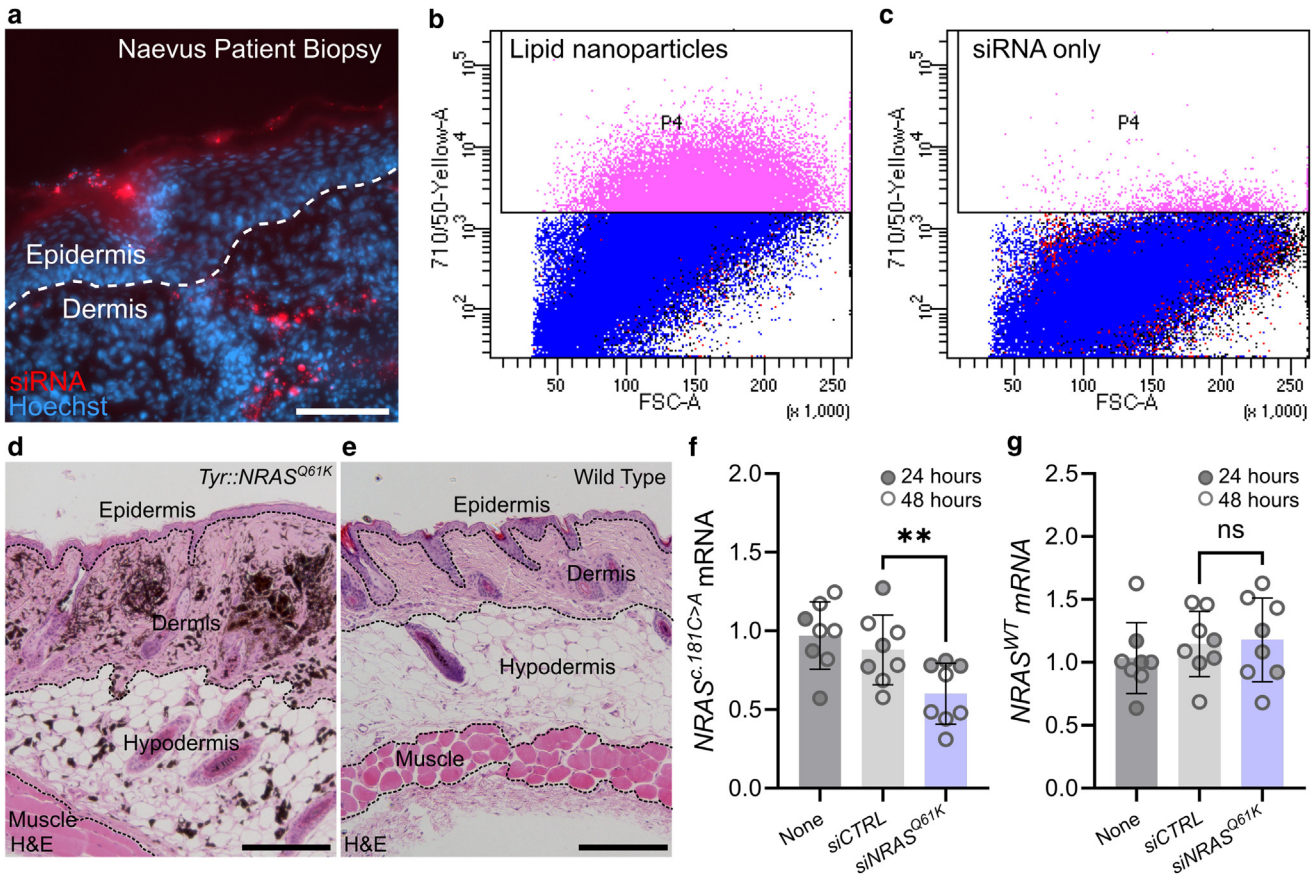

Figure 5. In vivo delivery and knockdown of nevus cell causing *NRAS* variant with si*NRAS*^{Q61K}-loaded lipid nanoparticles. (**a**) Intradermal injection of nevus patient biopsy with siRNA-cy5 encapsulated in lipid nanoparticles. Bar = 100 μm. (**b**) siRNA encapsulated in lipid nanoparticles could be delivered to the cells of the dermis of nevus patient biopsy. (**c**) siRNA not encapsulated in lipid nanoparticles delivered relatively little into the cells of the dermis of nevus patient biopsy. (**d**) Nevus-causing *NRAS* variant expression driven by the melanocyte-specific tyrosinase promoter causes ectopic pigment cells in the dermis and hypodermis of *Tyr::NRAS*^{Q61K} mice. Bar = 200 μm. (**e**) No ectopic pigment cells in the dermis or hypodermis of *NRAS*^{WT} mice. Bar = 200 μm. (**f**) Intradermal injection of *Tyr::NRAS*^{Q61K} mice with si*NRAS*^{Q61K} decreased the expression of nevus cell causing *NRAS* variant. (**g**) Intradermal injection of *Tyr::NRAS*^{Q61K} mice with si*NRAS*^{Q61K} did not decrease the expression of endogenous mouse *Nras*^{WT}. n = 8. Data were pooled together from 2 experiments. Points = individual mice (closed circles = mice treated for 24 hours, open circles = mice treated for 48 hours), bars = mean, and error bars = SD, with unpaired 1-tailed *t*-test (for **f** and **g**). FSC-A, forward scatter area; ns, not significant; siCTRL, control-targeted small interfering RNA; siRNA, small interfering RNA.

(*Tg*[*Tyr-NRAS*Q61K*]*1Bee*; MGI:3768645 [Ackermann et al, 2005]) (Supplementary Figure S8a), in which mice have hyperpigmented skin and an excess of melanin-producing cells present in the dermis (Figure 5d and e and Supplementary Figure S8b). Eight mice received 2 separate intradermal injections of si*NRAS*^{Q61K} RTNPs into the skin of the back, shaved just prior to the procedure, in addition to an identical neighboring injection of RTNPs containing nontargeting siRNA as a control. si*NRAS*^{Q61K} RTNPs induced knockdown of the transgenic variant *NRAS* allele (Figure 5f) but not of the WT endogenous *Nras* allele (Figure 5g) at 24 and 48 hours. No side effects were observable macroscopically either at the injection site or on mouse behavior or general health at this time point.

DISCUSSION

Cancer prevention is an area attracting increasing attention and research investment (Cancer Research UK, 2022–2023; Lopez, 2015). Cancer prevention has usually taken the form of lifestyle modifications, such as optimizing diet and exercise (Kohler et al, 2016), although notable therapeutic interventions such as eradication of *H pylori* to reduce the incidence of gastric cancer have been demonstrated to be effective (Choi et al, 2020). However, genetic therapies have not yet been used in the field of cancer prevention. We hypothesized that targeting oncogenic drivers in benign tumors with a predisposition to malignant transformation would not only treat the lesions themselves but serve as proof of concept for this therapeutic angle on cancer prevention. We chose to tackle CMN as an untreatable benign disease with severe morbidity, including progression to fatal childhood melanoma.

The characteristic pathology in this disease is a large number of nevus cells within the dermis, which persist throughout life. This is an unusual situation because melanocytic precursors usually migrate out of the dermis during embryogenesis into the dermal–epidermal junction, where there is thereafter exquisite regulation of numbers and spacing responsible for the uniformity of human skin pigmentation (Nordlund et al, 2007). Clinical observations of regrowth of partially resected nevi (Polubothu and Kinsler, 2020) implied that these cells were not persisting owing to

true senescence. Histological studies instead revealed that they were in a state of extremely low proliferation characterized by stem cell marker expression (Kinsler et al, 2013a), which we considered could be compatible with a RAS-induced quiescence or resistance to apoptosis. Agnostic to the exact mechanisms at the outset, we selected direct targeting of the causative variant as the best potential method to induce resolution of the lesions and indeed to study the mechanism itself.

Previous reports of *NRAS* knockdown by various RNA interference techniques in cancer cell lines have demonstrated that nonallele-specific targeting reduces proliferation (Burgess et al, 2014) and that targeting of the variant allele as opposed to the WT increases apoptosis (Eskandarpour et al, 2005). We demonstrate in this study that selective silencing of the variant *NRAS* allele is achievable in multiple samples of primary patient cells from benign melanocytic nevi. This leads to a reduction in NRAS protein levels, a downstream reduction in MAPK pathway activation, and a reduction in cellular proliferation rate. Successful protection of the siRNA from degradation and delivery into the dermis, combined with targeting to nevus cells, then allowed us to deliver this targeted nanomedicine into the skin of a humanized mouse model of CMN, where knockdown was demonstrated 48 hours after a single treatment.

In terms of mechanism, high baseline levels and significant suppression on siRNA treatment of *ARL6IP1* and *BIRC5* (survivin) point to induction of apoptosis. ARL6IP1 is located in the membrane of the ER where it protects the cell from apoptosis (Lui et al, 2003) and is important in the survival of tumor cells (Bishayee et al, 2022). Although not known to be downstream of *NRAS*, oncogenic NRAS activity has previously been demonstrated to drive resistance to ER stress (Bright et al, 2018), and inhibition of the MAPK pathway sensitizes human melanoma cells to ER stress–induced apoptosis (Jiang et al, 2007). In further support, our transcriptomic data also identified significant upregulation of *ERN1*, a key player in the same pathway. However, expressions of other notable genes associated with ER stress (ie, *EIF2AK3*, *ATF4*, *ATF6*, and *GRP78*) were unaffected, suggesting that ER stress may not be the only reason whereby si$NRAS^{Q61K}$ treatment results in the observed apoptosis.

Survivin is known to be highly expressed in cancers and to inhibit activation of caspases (Wheatley and Altieri, 2019). It is downstream of many apoptotic triggers, including ER stress (Gundamaraju et al, 2018). Expression in nonproliferating adult tissues (which would include CMN cells) has traditionally been considered to be very low (Wheatley and Altieri, 2019); however, in support of our findings, high baseline levels of survivin have previously been demonstrated in (acquired) melanocytic nevi (Florell et al, 2005). In further support, survivin expression is downstream of oncogenic RAS. With the development of the most targeted small-molecule therapy for oncogenic RAS, $KRAS^{G12C}$ inhibitor sotorasib (Amgen), elevated levels of survivin were identified as the mechanism of protection from apoptosis in pancreatic cancer cells (Chang et al, 2023). Our data demonstrating progression from the early induction of these apoptosis markers to high levels of caspase 3/7 raise the possibility that even transient suppression of variant *NRAS* expression within a disease cell may lead to irreversible triggering of the apoptotic cascade.

The comparison of the effects of treatment with si$NRAS^{Q61K}$ and MEKi trametinib alone and in combination is interesting. Although trametinib showed reduction in proliferation of CMN cells in culture within 24 hours of treatment, there was no triggering of apoptosis even over a prolonged period when given alone or in combination with control siRNA. However, the addition of trametinib to treatment with targeted siRNA led to a combinatorial effect on both proliferation and induction of apoptosis. Although si$NRAS^{Q61K}$ is therefore operating through downstream effectors in addition to the MAPK pathway, silencing of the variant allele also appears to permit additional activity of the MEKi.

RNA interference as a therapy has become a reality in clinical practice over the last 5 years since the first Food and Drug Administration approval in 2018 for Patisiran (Alnylam Therapeutics), and the initial concerns about lack of stability of this treatment modality have become more than refuted by treatments, which require only 1 administration every 6 months (Ray et al, 2020). Skin disease has not yet been tackled systematically in this way, but the findings in this study strongly support delivery and treatment directly into or onto the skin. Systemic or intrathecal dissemination is likely to be important for targeting of other aspects of the disease and remains to be explored. The use of variant allele-specific therapies and receptor targeting add specificity to the treatment, which should enable dose minimization, whereas the use of lipid nanoparticles appears in these studies to be sufficient to protect the siRNA from degradation in the short term. Backbone modifications of the siRNA are ongoing to stabilize the therapy without compromising targeting or effectiveness.

Taken together, these data show that protection from apoptosis is critically involved in persistence of *NRAS*-driven melanocytic nevi and that treatment with allele-specific siRNA removes that protection. Reversal of benign RAS-driven tumors could potentially form the basis of cancer prevention, particularly in high-risk individuals.

MATERIALS AND METHODS

Patient cohort

CMN nevus cells were cultured from 8 children with CMN who had been recruited to research after written informed consent and under London Bloomsbury Research Ethics Committee approvals 12/LO/1522 and 17/LO/1783 and where *NRAS* c.181C>A p.(Q61K) had been identified on genotyping. Skin samples were obtained either from surgical excision or from punch biopsy. Patient material was handled in compliance with the United Kingdom Human Tissue Act and the Declaration of Helsinki.

Culture of HCT116 cell lines

HCT116 colorectal carcinoma WT (CrownBio, C8052C-WT) and homozygous $NRAS^{c.181C>A;p.Q61K}$ (CrownBio, C6072C) cells were cultured in McCoy's 5a Medium (ATCC, 30-2007) containing 10% fetal bovine serum.

Isolation and culture of primary CMN nevus cells

Skin biopsies were processed in the laboratory within 2 hours of collection. The hypodermis was removed before the dermis/epidermis was incubated in a solution of PluriSTEM Dispase II

(Sigma-Aldrich, SCM133) containing 2.5 mM calcium chloride dihydrate (Sigma-Aldrich, C7902) and 1.5 U/ml Collagenase D (Roche, 11088858001) at 37 °C. After partial digestion, the epidermis was separated from the dermis with forceps to continue digestion of both components in separate tubes. When the tissues were adequately digested, they were resuspended in 5 ml Ham F-10 nutrient mix (Thermo Fisher Scientific, 11550043) before separation through a 40-μm cell strainer (Corning, 431750) to remove aggregate material. The cells were pelleted at 250*g* for 5 minutes.

The dermis-derived cells and epidermis-derived cells were separately resuspended in nevus cell growth medium (Supplementary Table S2). Cells were seeded onto tissue culture–treated plastic, and media were changed every 3–4 days. When cells approached 70–80% confluency, they were dissociated with Accutase (Sigma-Aldrich, A6964) and reseeded at a lower density. All cultures were incubated in a typical humidified, 37 °C, 5% carbon dioxide incubator.

Live imaging

Cells were seeded into #1.5 high-performance cover glass bottomed 24-well plates (Cellvis, P24-1.5H-N) at a density of 5,263 cells per cm^2 (10,000 cells per well) in 500 μl media. Imaging was carried out on the Livecyte 2 imaging system (Phasefocus) 24 hours after seeding the cells. The images were acquired with the ×10 objective at 10-minute intervals. Images were processed and analyzed with Phasefocus Cell Analysis Toolbox software. For the live apoptosis assay, cells were imaged using the Incucyte Live Cell Analysis System. Cells were cultured with 5 μM of caspase 3/7 substrate (Biotium, 10402). Measurements were taken every 3 hours. The first measurement was omitted because condensation disrupted imaging. Analysis was performed using the incucyte's basic analyser, from which raw data were exported.

Flow cytometry

Cells were analyzed by flow cytometry using the Amnis ImageStream flow cytometer to analyze the cell cycle on the basis of DNA content (DAPI intensity) and the Aria III cell sorter for measure delivery of siRNA to CMN tissue.

Immunocytochemistry

Nevus cells were washed once with Dulbecco's PBS and fixed with 4% paraformaldehyde for 20–30 minutes at room temperature before washing with Dulbecco's PBS. Cells were incubated in blocking buffer (Supplementary Table S3) for 1 hour. They were then incubated with primary antibodies (Supplementary Table S3) prepared in blocking buffer. A minimum of 60 μl/well of 96-well plate, overnight at 4 °C, was used. After washes in Dulbecco's PBS, the cells were incubated with secondary antibodies (Supplementary Table S3) for 2 hours at room temperature. During the final series of Dulbecco's PBS washes, cells were incubated with 1 μg/ml Hoechst 33342 in Dulbecco's PBS.

siRNA design and optimization

A walked-design panel of 19 21mer (including TT overhang) siRNAs centred on and targeting the variant *NRAS* mRNA transcript (c.181C>A) was custom made from Sigma-Aldrich (Supplementary Table S4). ON-TARGETplus nontargeting control pool (Horizon, D-001810-10-50) was used as a scrambled control. siRNAs were optimized using paired parental C8052C-WT and homozygous *NRAS* (c.181C>A; p.Q61K) (C6072C) HCT116 colorectal carcinoma cell line (CrownBio) before testing on nevus cell cultures. Unless otherwise stated, cells were transfected by siRNA in their normal media using Lipofectamine RNAiMAX (Thermo Fisher Scientific, 13778075) according to the manufacturer's instructions.

In silico evaluation of allelic discrimination

Two formulae were used to assess siRNA candidates for likely allelic discrimination, one tolerating the targeting of the nontarget allele and the other not, as per previously published methods (Takahashi and Hohjoh, 2014).

qPCR

RNA was extracted (Qiagen, 74134), and cDNA was synthesized (Applied Biosystems, 4368814). Reactions were set up using PowerUP SYBR Green Master Mix (Applied Biosystems, A25742) or Taqman Universal PCR Master Mix (Applied Biosystems, 4304437) according to the manufacturer's formulation with appropriate primers/Taqman assays (Supplementary Table S1). The qPCR protocol was initiated with 50 °C for 2 minutes and 95 °C for 10 minutes, followed by 40 cycles of 95 °C for 15 seconds and 60 °C for 1 minute. The qPCR was performed using the QuantStudio 7 Flex Real-Time PCR System (Applied Biosystems). Relative expression values ($2^{-\Delta\Delta Ct}$) were calculated with normalization to *GAPDH* expression. Data presented in figures are normalized to the mean value of untreated cells per tissue.

Western blot

Protein was extracted in lysis buffer (150 mM sodium chloride, 1% Triton X-100, 50 mM Tris pH8, 1 μM phenylmethylsulfonyl fluoride, 1× protease inhibitor cocktail [Roche, 11836153001], 1× phosphatase inhibitor cocktail [Roche, 04906837001]). Protein was prepared in Laemmli buffer containing 12.5 mM dithiothreitol before denaturation at 90 °C for 10 minutes. Sample was loaded into Mini-PROTEAN TGX gels and run at 100 V until proteins of interest were appropriately resolved. Protein was transferred onto Immobolin-FL Transfer Membrane (Merck, IPFL00005) with Towbin Buffer (25 mM Tris, 192 mM glycine, 20% methanol) using StandardSD Bio-Rad protocol (25V-1A-30 minutes) on the Trans-Blot Turbo Transfer System (Bio-Rad Laboratories). Membranes were blocked for 1 hour in appropriate buffers for antibody/imaging method (Supplementary Table S5). Primary antibodies were incubated with the membrane in the blocking buffer overnight at 4 °C with agitation. Secondary antibodies were incubated with the membrane for 2 hours at room temperature with agitation. Blots were imaged with Clarity Western ECL substrate (Bio-Rad Laboratories, 170-5060) using Gel Doc System (Bio-Rad Laboratories) for horseradish peroxidase–conjugated secondary antibodies or the Odyssey CLx (LI-COR Biosciences) for IRDye-conjugated secondary antibodies (Supplementary Table S5). The intensity of protein bands was quantified using the gel analysis tool on FIJI. Protein levels were normalized to those of vinculin.

Receptor-targeted lipid nanoparticles

Lipids for cationic nanoparticles were resuspended and mixed to a total lipid concentration of 1 mg/ml in 100% ethanol: 49.5% cationic lipid DOTMA (DOTMA 1,2-di-O-octadecenyl-3-trimethylammonium propane [chloride salt]). Molecular weight: 670.575 (CAS: 104872-42-6; Avanti SKU: 890898P); 49.5% neutral lipid DOPE (18:1 [Δ9-Cis] PE [DOPE] 1,2-dioleoyl-sn-glycero-3-phosphoethanolamine. Molecular weight: 744.034 [CAS:4004-05-1; Avanti SKU: 850725P]). 1% PEGylated lipid (DPPE-PEG[2000] Azide 1,2-dipalmitoyl-sn-glycero-3-phosphoethanolamine-N-azido [polyethylene glycol])-2000 (ammonium salt). Molecular weight: 2760.38 (CAS: not available; Avanti SKU: 880231P). Peptide

(27 amino acids, Lys-Lys-Lys-Lys-Lys-Lys-Lys-Lys-Lys-Lys-Lys-Lys-Lys-Lys-Lys-Gly-Ala-Cys-Ile-Ser-Val-Tyr-Met-Met-Cys-Gly (KKKKKKKKKKKKKKKKGACISVYMMCG [AMSBIO, custom request]) is resuspended to a concentration of 10 mg/ml in 95% ethanol.

Self-assembly of lipid nanoparticles was initiated by mixing the lipids, peptide, and siRNA in that order and, unless otherwise specified, at a ratio of 1:4:1 (lipid:peptide:siRNA). A total of 3 volumes of water must be used for every 1 volume of ethanol (ie, input of siRNA must be in 3 volumes of water for every 1 volume of ethanol from the lipid and peptide stock). The lipid nanoparticles containing siRNA were dialyzed (GeBaFlex-tube − Dialysis kit MWCO 8 kDa, Generon) to exchange the ethanol to water, changing the water 3 times over 24 hours.

The RTNPs were concentrated by loading the dialyzed sample in Centrifugal filter units (Amicron Ultra, Merck) and centrifugation at speed/time outlined in protocol. The concentrated nanoparticles were resuspended in sucrose solution (275-300 mOsm) and sterile filter (Syringe Filter PTFE 25 mm 0.2 ulm NSTR, Thermo Fisher Scientific, 15141499).

The hydrodynamic size and charge of lipid nanoparticles were measured with the Malvern Zetasizer. RNase protection assay was performed by treating the formulated lipid nanoparticles or siRNA alone with RNase A at 2 μg/ml before incubation for either 1, 2, or 4 hours at 37 °C. A total of 1 μl of RNase inhibitor was added to stop the digestion. The nanoparticles were then lysed with 16.4 mM of SDS before running on an agarose gel. The encapsulation assay was performed by loading formulated lipid nanoparticles into an agarose gel and checking for free siRNA after electrophoresis.

Animals

All animal studies were approved by the Francis Crick Institute's Animal Welfare and Ethical Review Body and licensed under UK Home Office regulations. Tyr::NRASQ61K mice (*Tg*[Tyr-NRAS*Q61K]*1Bee;* MGI:3768645 [Ackermann et al, 2005]) were supplied from the European Mouse Mutant Archive. Genetically modified mouse testing on rederived progeny showed close to inbred and a mixture of background strain groups C57BL/6 and the substrains C57BL/6J and C57BL/6JOlaHsd. Secondary background of DBA/2 was also detected. Mouse phenotype and health were consistent with previous published reports, having uniformly black skin, including ears, paws, and tail. No mouse developed melanoma during the duration of the study.

In vivo delivery of lipid nanoparticles to Tyr::NRASQ61K mice

Tyr::NRASQ61K mice (aged 41−45 weeks, 3 females, 5 males) were shaved with clippers before receiving intradermal injections (insulin needle 30G) of 450 μg of RTNPs prepared in sucrose solution (295 mOsmol) on either side of the dorsal midline while under general anaesthesia (isolfurane). Injection sites were marked by drawing around the bleb with a marker pen. Forty-eight hours later, the mice were culled, and a 4-mm punch biopsy was collected from each site. The biopsy was stored in RNAlater (Invitrogen, AM7021) prior to RNA extraction.

RNAseq

Two separate RNAseq experiments were run, the first for HCT116 cells and the second for primary nevus cells. HCT116 cells were treated with siRNA-targeted control (n = 3), siRNA1 (n = 3), siRNA8 (n = 3), or siRNA15 (n = 3). Patient (n = 7) nevus cells were each treated with siRNA-targeted control or si$NRAS^{Q61K}$ (siRNA8) or no treatment. Total RNA was extracted from cells using the AllPrep DNA/RNA Mini Kit (Qiagen). cDNA libraries were prepared using the KAPA 12 mRNA HyperPrep Kit (Roche) and subsequently sequenced on a NextSeq 500 sequencer 13 (paired end) (Illumina). Fastq files were processed by fastp (0.20.0) and aligned to the human genome (Ensembl, GRCh 38.109) using STAR (2.7.9a). The uniquely mapped read counts matrix was obtained using featureCounts (Rsubsead 1.6.4), and differential expression analysis was performed using DESeq2 (1.38.3). Adjusted *P*-values were collected with Benjamini−Hochberg correction. Principal component analysis plot was generated using functions included in the same package.

Statistical analysis

Statistical analyses were carried out as described in each figure using either a *t*-test or ANOVA. Corrections for multiple comparisons (Tukey, Bonferroni, or Šidák) were done by selecting the recommended option on GraphPad Prism. Adjusted *P*-values (Benjamini−Hochberg correction) were used with RNAseq data. Nonstatistically significant difference = $P > .05$. Statistically significant difference = $^{*}P \leq .05$ and $^{**}P \leq .01$.

DATA AVAILABILITY STATEMENT

Datasets related to this article can be found at ArrayExpress (https://www.ebi.ac.uk/biostudies/arrayexpress), hosted with accession number E-MTAB-13221.

ORCIDs

Dale Bryant: http://orcid.org/0000-0002-4783-4796
Sara Barberan-Martin: http://orcid.org/0000-0003-0142-4078
Ruhina Maeshima: http://orcid.org/0000-0003-1473-9757
Ignacio del Valle Torres: http://orcid.org/0000-0003-2595-3652
Mohammad Rabii: http://orcid.org/0000-0002-1605-6143
William Baird: http://orcid.org/0009-0001-7746-7042
Aimie Sauvadet: http://orcid.org/0000-0002-8980-1239
Charalambos Demetriou: http://orcid.org/0000-0001-6630-1322
Phoebe Jones: http://orcid.org/0009-0008-2910-8863
Nicole Knöpfel: http://orcid.org/0000-0002-6438-6550
Fanourios Michailidis: http://orcid.org/0000-0002-0408-3603
Melissa Riachi: http://orcid.org/0000-0001-7278-1780
Dorothy C. Bennett: http://orcid.org/0000-0002-3639-7527
Davide Zecchin: http://orcid.org/0000-0002-4784-0336
Alan Pittman: http://orcid.org/0000-0002-8112-2987
Satyamaanasa Polubothu: http://orcid.org/0000-0001-7195-5670
Stephen Hart: http://orcid.org/0000-0001-8254-376X
Veronica A. Kinsler: http://orcid.org/0000-0001-6256-327X

CONFLICT OF INTEREST

The authors state no conflict of interest. Patent application number GB2216028.7 has been filed in relation to this work on behalf of DB and VAK.

ACKNOWLEDGMENTS

We gratefully acknowledge the participation of the patients and families in this research. We gratefully acknowledge the support and expertise of the United Kingdom National Institute of Health and Care Research grant steering committee: Jane White (University College London/Crick, chair), Lionel Larue (Curie Institute), Gudrun Moore (University College London), Nick Reynolds (Newcastle University), and Francesco Muntoni (University College London). VAK and DB are funded by a United Kingdom National Institute of Health and Care Research Research (NIHR) Professorship (grant NIHR300774). This project was supported by NIHR300774, Caring Matters Now Charity, and the LifeArc-Crick Fund. The work was supported by the GOSHCC Livingstone Skin Research Centre and by the NIHR through the Biomedical Research Centre at Great Ormond Street Hospital for Children NHS Foundation Trust and the UCL Great Ormond Street Institute of Child Health. Research support was provided by the Crick Science Technology Platforms: advanced light microscopy, advanced sequencing, biological research facility, experimental histopathology, flow cytometry, high-throughput screening, and structural biology.

AUTHOR CONTRIBUTIONS

Conceptualization: VAK; Data Curation: IdVT, AP; Formal Analysis: DB, WB, CD, MRa, VK; Funding Acquisition: VAK; Investigation: DB, SB, MRa, MRi, WB, CD, DZ, FM, PJ, NK, SP; Methodology: SP, DCB, RM, SH, AS; Project Administration: VAK; Resources: NK, RM, SH; Supervision: SH, VAK; Visualization: DB; Writing — Original Draft Preparation: DB, VAK; Writing — Review and Editing: VAK

SUPPLEMENTARY MATERIAL

Supplementary material is linked to the online version of the paper at www.jidonline.org, and at https://doi.org/10.1016/j.jid.2024.04.031.

REFERENCES

Ackermann J, Frutschi M, Kaloulis K, McKee T, Trumpp A, Beermann F. Metastasizing melanoma formation caused by expression of activated N-RasQ61K on an INK4a-deficient background. Cancer Res 2005;65:4005–11.

Al-Olabi L, Polubothu S, Dowsett K, Andrews KA, Stadnik P, Joseph AP, et al. Mosaic RAS/MAPK variants cause sporadic vascular malformations which respond to targeted therapy [published correction appears in J Clin Invest 2018;128:1496–508]. J Clin Invest 2018;128:5185.

Alper JC, Holmes LB. The incidence and significance of birthmarks in a cohort of 4,641 newborns. Pediatr Dermatol 1983;1:58–68.

Bishayee K, Habib K, Nazim UM, Kang J, Szabo A, Huh SO, et al. RNA binding protein HuD promotes autophagy and tumor stress survival by suppressing mTORC1 activity and augmenting ARL6IP1 levels [published correction appears in J Exp Clin Cancer Res 2022;41:52]. J Exp Clin Cancer Res 2022;41:18.

Bourdeaut F, Hérault A, Gentien D, Pierron G, Ballet S, Reynaud S, et al. Mosaicism for oncogenic G12D KRAS mutation associated with epidermal nevus, polycystic kidneys and rhabdomyosarcoma. J Med Genet 2010;47:859–62.

Bright MD, Clarke PA, Workman P, Davies FE. Oncogenic RAC1 and NRAS drive resistance to endoplasmic reticulum stress through MEK/ERK signalling. Cell Signal 2018;44:127–37.

Burgess MR, Hwang E, Firestone AJ, Huang T, Xu J, Zuber J, et al. Preclinical efficacy of MEK inhibition in Nras-mutant AML. Blood 2014;124:3947–55.

Cancer Research UK. Cancer Research UK prevention research strategy; 2022–2023.

Castilla EE, da Graça Dutra M, Orioli-Parreiras IM. Epidemiology of congenital pigmented naevi: I. Incidence rates and relative frequencies. Br J Dermatol 1981;104:307–15.

Chang WH, Liu Y, Hammes EA, Bryant KL, Cerione RA, Antonyak MA. Oncogenic RAS promotes MYC protein stability by upregulating the expression of the inhibitor of apoptosis protein family member survivin. J Biol Chem 2023;299:102842.

Choi IJ, Kim CG, Lee JY, Kim YI, Kook MC, Park B, et al. Family history of gastric cancer and Helicobacter pylori treatment. N Engl J Med 2020;382:427–36.

Dos Santos W, Dos Reis MB, Porto J, de Carvalho AC, Matsushita M, Oliveira G, et al. Somatic targeted mutation profiling of colorectal cancer precursor lesions. BMC Med Genomics 2022;15:143.

Eskandarpour M, Kiaii S, Zhu C, Castro J, Sakko AJ, Hansson J. Suppression of oncogenic NRAS by RNA interference induces apoptosis of human melanoma cells. Int J Cancer 2005;115:65–73.

Etchevers HC, Rose C, Kahle B, Vorbringer H, Fina F, Heux P, et al. Giant congenital melanocytic nevus with vascular malformation and epidermal cysts associated with a somatic activating mutation in BRAF. Pigment Cell Melanoma Res 2018;31:437–41.

Florell SR, Bowen AR, Hanks AN, Murphy KJ, Grossman D. Proliferation, apoptosis, and survivin expression in a spectrum of melanocytic nevi. J Cutan Pathol 2005;32:45–9.

Groesser L, Herschberger E, Ruetten A, Ruivenkamp C, Lopriore E, Zutt M, et al. Postzygotic HRAS and KRAS mutations cause nevus sebaceous and Schimmelpenning syndrome. Nat Genet 2012;44:783–7.

Gundamaraju R, Vemuri R, Chong WC, Myers S, Norouzi S, Shastri MD, et al. Interplay between endoplasmic reticular stress and survivin in colonic epithelial cells. Cells 2018;7:171.

Hafner C, Toll A, Real FX. HRAS mutation mosaicism causing urothelial cancer and epidermal nevus. N Engl J Med 2011;365:1940–2.

Happle R. Lethal genes surviving by mosaicism: a possible explanation for sporadic birth defects involving the skin. J Am Acad Dermatol 1987;16:899–906.

Jacobs AH, Walton RG. The incidence of birthmarks in the neonate. Pediatrics 1976;58:218–22.

Jiang CC, Chen LH, Gillespie S, Wang YF, Kiejda KA, Zhang XD, et al. Inhibition of MEK sensitizes human melanoma cells to endoplasmic reticulum stress-induced apoptosis. Cancer Res 2007;67:9750–61.

Kakiuchi N, Ogawa S. Clonal expansion in non-cancer tissues. Nat Rev Cancer 2021;21:239–56.

Kakiuchi N, Yoshida K, Uchino M, Kihara T, Akaki K, Inoue Y, et al. Frequent mutations that converge on the NFKBIZ pathway in ulcerative colitis. Nature 2020;577:260–5.

Kinsler VA, Anderson G, Latimer B, Natarajan D, Healy E, Moore GE, et al. Immunohistochemical and ultrastructural features of congenital melanocytic naevus cells support a stem-cell phenotype. Br J Dermatol 2013a;169:374–83.

Kinsler VA, Boccara O, Fraitag S, Torrelo A, Vabres P, Diociaiuti A. Mosaic abnormalities of the skin: review and guidelines from the European Reference Network for rare skin diseases. Br J Dermatol 2020;182:552–63.

Kinsler VA, O'Hare P, Bulstrode N, Calonje JE, Chong WK, Hargrave D, et al. Melanoma in congenital melanocytic naevi. Br J Dermatol 2017a;176:1131–43.

Kinsler VA, O'Hare P, Jacques T, Hargrave D, Slater O. MEK inhibition appears to improve symptom control in primary NRAS-driven CNS melanoma in children. Br J Cancer 2017b;116:990–3.

Kinsler VA, Thomas AC, Ishida M, Bulstrode NW, Loughlin S, Hing S, et al. Multiple congenital melanocytic nevi and neurocutaneous melanosis are caused by postzygotic mutations in codon 61 of NRAS. J Invest Dermatol 2013b;133:2229–36.

Kohler LN, Garcia DO, Harris RB, Oren E, Roe DJ, Jacobs ET. Adherence to diet and physical activity cancer prevention guidelines and cancer outcomes: a systematic review. Cancer Epidemiol Biomarkers Prev 2016;25:1018–28.

Küsters-Vandevelde HV, Willemsen AE, Groenen PJ, Küsters B, Lammens M, Wesseling P, et al. Experimental treatment of NRAS-mutated neurocutaneous melanocytosis with MEK162, a MEK-inhibitor. Acta Neuropathol Commun 2014;2:41.

Lopez G. Investing in cancer prevention and control to reduce global economic burden. https://connection.asco.org/blogs/investing-cancer-prevention-and-control-reduce-global-economic-burden; 2015. (accessed January 4, 2024).

Lui HM, Chen J, Wang L, Naumovski L. ARMER, apoptotic regulator in the membrane of the endoplasmic reticulum, a novel inhibitor of apoptosis. Mol Cancer Res 2003;1:508–18.

Marotta V, Bifulco M, Vitale M. Significance of RAS mutations in thyroid benign nodules and non-medullary thyroid cancer. Cancers (Basel) 2021;13:3785.

Martin SB, Polubothu S, Bruzos AL, Kelly G, Horswell S, Sauvadet A, et al. Mosaic BRAF fusions are a recurrent cause of congenital melanocytic nevi targetable by MAPK pathway inhibition. J Invest Dermatol 2024;144:593–600.e7.

Martincorena I, Roshan A, Gerstung M, Ellis P, Van Loo P, McLaren S, et al. Tumor evolution. High burden and pervasive positive selection of somatic mutations in normal human skin. Science 2015;348:880–6.

Martins da Silva V, Martinez-Barrios E, Tell-Martí G, Dabad M, Carrera C, Aguilera P, et al. Genetic abnormalities in large to giant congenital Nevi: beyond NRAS mutations. J Invest Dermatol 2019;139:900–8.

Masnari O, Neuhaus K, Aegerter T, Reynolds S, Schiestl CM, Landolt MA. Predictors of health-related quality of life and psychological adjustment in children and adolescents with congenital melanocytic nevi: analysis of parent reports. J Pediatr Psychol 2019;44:714–25.

Mir A, Agim NG, Kane AA, Josephs SC, Park JY, Ludwig K. Giant congenital melanocytic nevus treated with trametinib. Pediatrics 2019;143:e20182469.

Molina-Arcas M, Samani A, Downward J. Drugging the undruggable: advances on RAS targeting in cancer. Genes (Basel) 2021;12:899.

Nanki K, Fujii M, Shimokawa M, Matano M, Nishikori S, Date S, et al. Somatic inflammatory gene mutations in human ulcerative colitis epithelium. Nature 2020;577:254–9.

Nordlund JJ, Boissy RE, Hearing VJ, King TA, Oetting WS, Ortonne JP. The pigmentary system: physiology and pathophysiology. second edition. Oxford: Blackwell Publishing Ltd; 2007.

Polubothu S, Kinsler VA. Final congenital melanocytic naevi colour is determined by normal skin colour and unaltered by superficial removal techniques: a longitudinal study. Br J Dermatol 2020;182:721–8.

Polubothu S, McGuire N, Al-Olabi L, Baird W, Bulstrode N, Chalker J, et al. Does the gene matter? Genotype-phenotype and genotype-outcome associations in congenital melanocytic naevi. Br J Dermatol 2020;182:434–43.

Ray KK, Wright RS, Kallend D, Koenig W, Leiter LA, Raal FJ, et al. Two Phase 3 trials of Inclisiran in patients with elevated LDL cholesterol. N Engl J Med 2020;382:1507–19.

Reshetnyak AV, Nelson B, Shi X, Boggon TJ, Pavlenco A, Mandel-Bausch EM, et al. Structural basis for KIT receptor tyrosine kinase inhibition by antibodies targeting the D4 membrane-proximal region. Proc Natl Acad Sci U S A 2013;110:17832–7.

Salgado CM, Basu D, Nikiforova M, Bauer BS, Johnson D, Rundell V, et al. BRAF mutations are also associated with neurocutaneous melanocytosis and large/giant congenital melanocytic nevi. Pediatr Dev Pathol 2015;18:1–9.

Tagalakis AD, Lee DH, Bienemann AS, Zhou H, Munye MM, Saraiva L, et al. Multifunctional, self-assembling anionic peptide-lipid nanocomplexes for targeted siRNA delivery. Biomaterials 2014;35:8406–15.

Takahashi M, Hohjoh H. A novel measurement of allele discrimination for assessment of allele-specific silencing by RNA interference. Mol Biol Rep 2014;41:7115–20.

Tang J, Fewings E, Chang D, Zeng H, Liu S, Jorapur A, et al. The genomic landscapes of individual melanocytes from human skin. Nature 2020;586:600–5.

Uhlén M, Fagerberg L, Hallström BM, Lindskog C, Oksvold P, Mardinoglu A, et al. Proteomics. Tissue-based map of the human proteome. Science 2015;347:1260419.

van Laethem JL. Ki-ras oncogene mutations in chronic pancreatitis: which discriminating ability for malignant potential? Ann N Y Acad Sci 1999;880:210–8.

Wheatley SP, Altieri DC. Survivin at a glance. J Cell Sci 2019;132:jcs223826.

Zhou Y, Zhou B, Pache L, Chang M, Khodabakhshi AH, Tanaseichuk O, et al. Metascape provides a biologist-oriented resource for the analysis of systems-level datasets. Nat Commun 2019;10:1523.

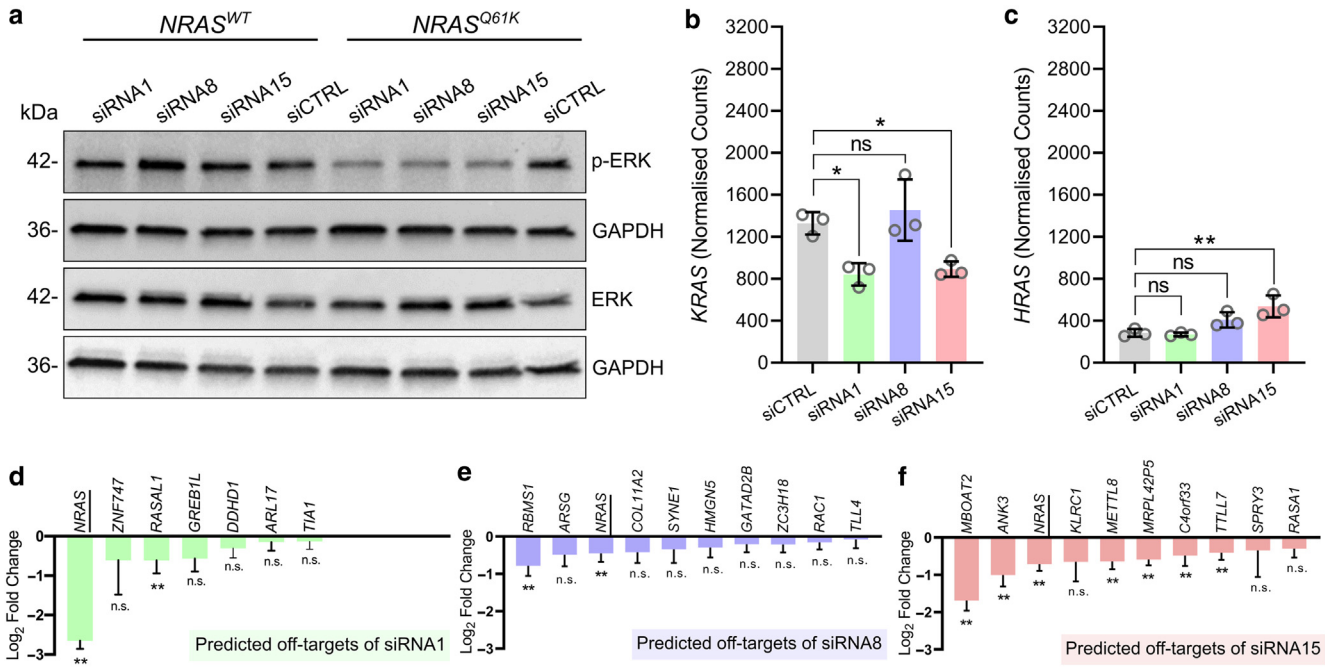

Supplementary Figure S1. Impact of siRNA candidates on MAPK activation and *NRAS* homologs in HCT116 cells. (**a**) siRNA candidates decrease p-ERK in the *NRAS* variant cell line (c.181C>A, $NRAS^{Q61K}$) compared with that in the *NRAS* WT cell line (c.181C, $NRAS^{WT}$). Total ERK and GAPDH are included as comparative loading controls. (**b, c**) Impact of 48-hour siRNA candidate treatment on homolog (**b**) *KRAS* and (**c**) *HRAS* in HCT116 cells (c.181C, $NRAS^{WT}$). (**d**–**f**) Impact of siRNA candidates on genes containing sequences with similarity to the target sequence of (**d**) siRNA1, (**e**) siRNA8, and (**f**) siRNA15 (*$P \leq .05$ and **$P \leq .1$). n = 3, bars = mean, and error bars = SEM, with ANOVA. ERK, extracellular signal–regulated kinase; ns, not significant; p-ERK, phosphorylated extracellular signal–regulated kinase; siCTRL, control-targeted small interfering RNA; siRNA, small interfering RNA; WT, wild-type.

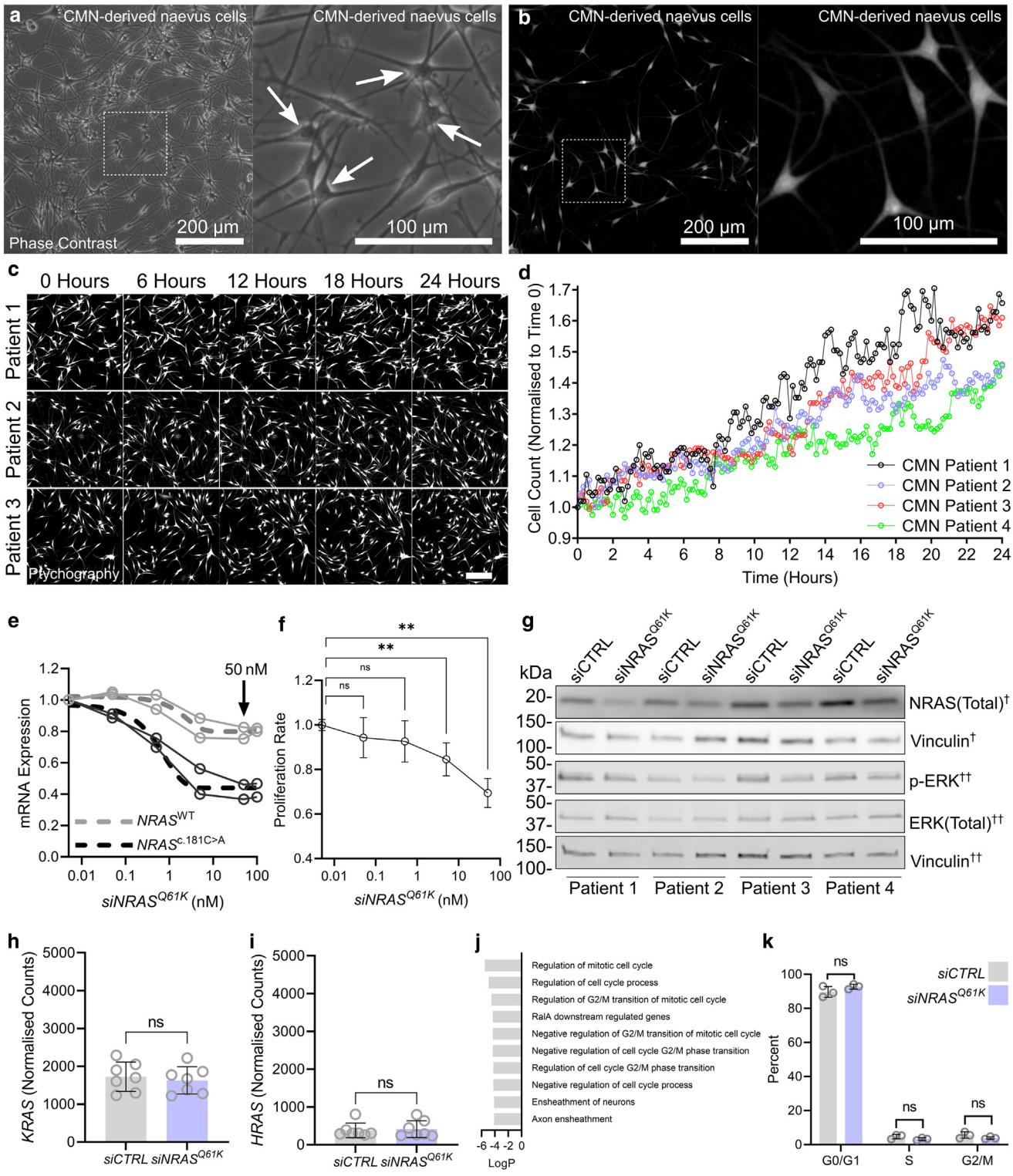

Supplementary Figure S2. Targeting *NRAS* variant in nevus cells from the tissue of patients with CMN. (**a**) Nevus cells cultured in feeder-free conditions imaged with phase contrast. Bar = 200 µm. (**b**) Ptychographic processing of phase contrast data provides high-contrast images that lend themselves to segmentation. Bar = 200 µm. (**c**) Ptychographic images of patient cell lines over 24 hours. Bar = 200 µm. (**d**) Cell counts using ptychographic images of patient cell lines over 24 hours normalized to time 0, demonstrating a degree of interpatient variability in growth rate as expected from primary cultures. (**e**) Dose-dependent effects on $NRAS^{WT}$ (gray) and $NRAS^{c.181C>A}$ (black) transcript expression after 48 hours of treatment of nevus cells with different concentrations of siRNA8 ($siNRAS^{Q61K}$). RNAiMAX was used as the delivery vector, and the arrow is the concentration suggested in the manufacturer's instructions. Two patient-derived nevus cell lines were tested (individual circles at each time point), with the perforated line representing the mean of the 2. (**f**) Dose-dependent effects of $siNRAS^{Q61K}$ treatment on proliferation (48 hours). (**g**) Western blot of protein lysates collected from all nevus patient cell cultures treated with siCTRL or $siNRAS^{Q61K}$ for 48 hours. All images are from the same blot. †Chemiluminescence imaging was required to detect NRAS protein levels because it was more sensitive than the Odyssey. ††The Odysee (fluorescence) was required to assess pERK levels because it permitted simultaneous measurement of total ERK and pERK using secondary antibodies conjugated to fluorophores of different wavelengths. (**h, i**) Impact of 48-hour $siNRAS^{Q61K}$ treatment of nevus cells on *NRAS*

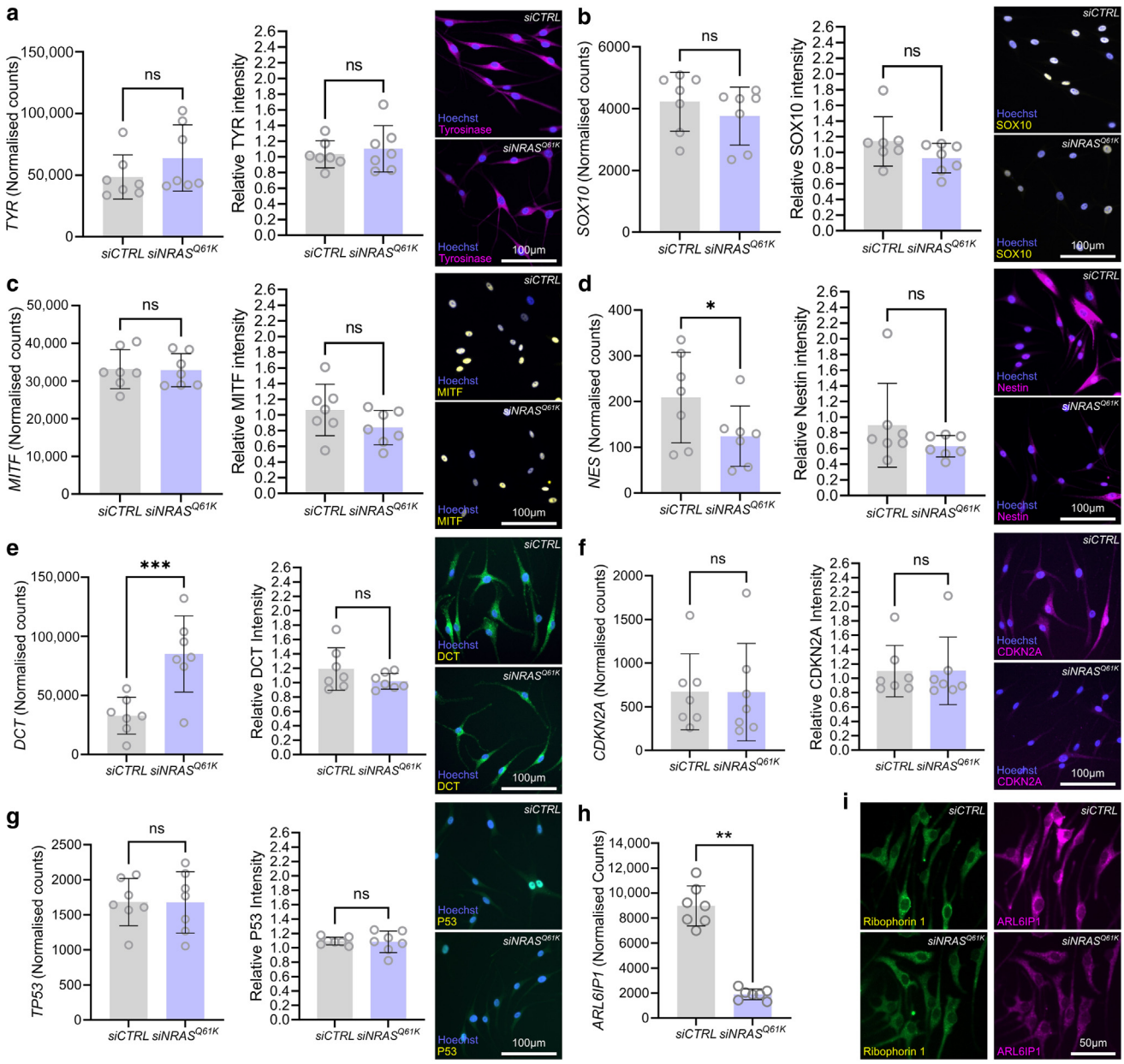

Supplementary Figure S3. Gene expression and antibody reactivity to nevus cells (*NRAS c.181C>A (p.Q61K)* treated with *siNRAS^{Q61K}* for 48 hours. RNAseq data (normalized counts) and relative signal intensity from antibody reactivity for (**a**) TYR, (**b**) SOX10, (**c**) MITF, (**d**) NES, (**e**) DCT, (**f**) CDKN2A, (**g**) p53, and (**h**) *ARL6IP1* (note quantification of ARL6IP1 antibody reactivity is in the main text). n = 7 (individual values). Bars = mean, and error bars = SD, with paired *t*-test. (**i**) Immunocytochemistry showing decreased ARL6IP1 (magenta) expression in response to 48-hour *siNRAS^{Q61K}* treatment. ARL6IP1 was assessed alongside an antibody targeting ribophorin 1 (endoplasmic reticulum, green). (**a**–**g**) Bar = 200 µm, (**i**) bar = 50 µm. ns, not significant; RNAseq, RNA sequencing; siCTRL, control-targeted small interfering RNA.

homologs (**h**) *KRAS* and (**i**) *HRAS*. (**j**) Top 10 enriched pathways from genes with expression changed (criteria: >1 fold; ≤1 fold; $P \leq .05$) by 48 hours *siNRAS^{Q61K}* treatment of nevus cells. (**k**) Fraction of nevus cells in each stage of the cell cycle (estimated on the basis of DNA content) after 48-hour *siNRAS^{Q61K}* treatment. CMN, congenital melanocytic nevus; ERK, extracellular signal–regulated kinase; ns, not significant; pERK, phosphorylated extracellular signal–regulated kinase; siCTRL, control-targeted small interfering RNA; siRNA, small interfering RNA.

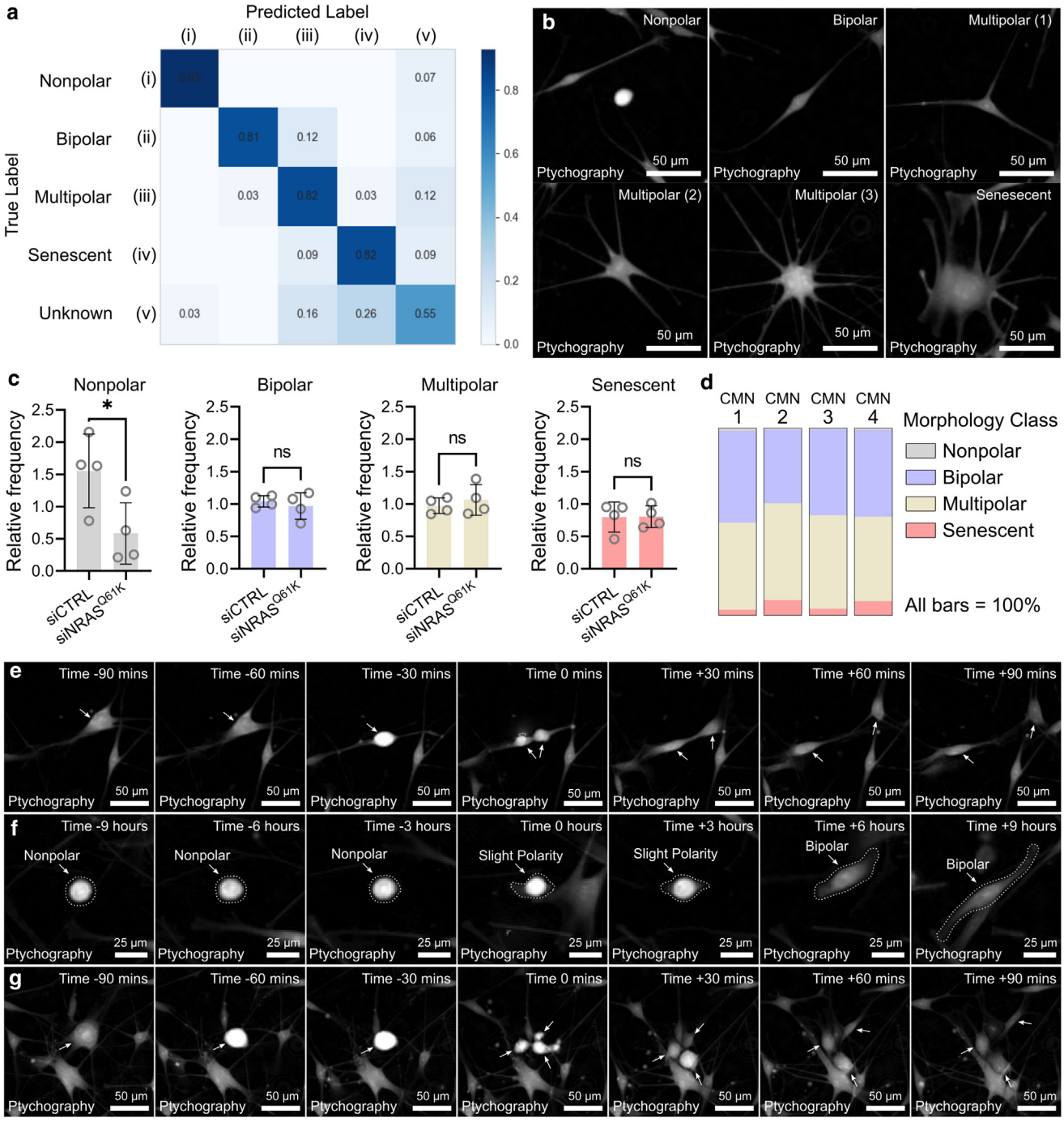

Supplementary Figure S4. Classification of nevus cell morphologies. (**a**) Evaluation of classification tool presented as a confusion matrix. (**b**) Increasing multipolar nevus cell morphologies (multipolar 1−3) were considered as a single category in the analysis to improve accuracy of the classification tool. Bar = 50 µm. (**c**) Treatment of nevus cells with *siNRAS*^{Q61K} (48 hours) decreases nonpolar cells. n = 4. Bars = mean, and error bars = SD, with 1-tailed paired *t*-test. (**d**) Comparable fractions of each cell morphology for 4 different CMN patient cell lines. (**e**) Ptychographic images over 3 hours, during which a cell divides (time 0). Bar = 50 µm. (**f**) Ptychographic images over 18 hours, during which a perpetual (at least 9 hours) nonpolar nevus cell becomes polar (time 0). Bar = 25 µm. (**g**) Ptychographic images over 3 hours, during which a single cell becomes 3 daughter cells (time 0). Bar = 50 µm. CMN, congenital melanocytic nevus; min, minute; siCTRL, control-targeted small interfering RNA.

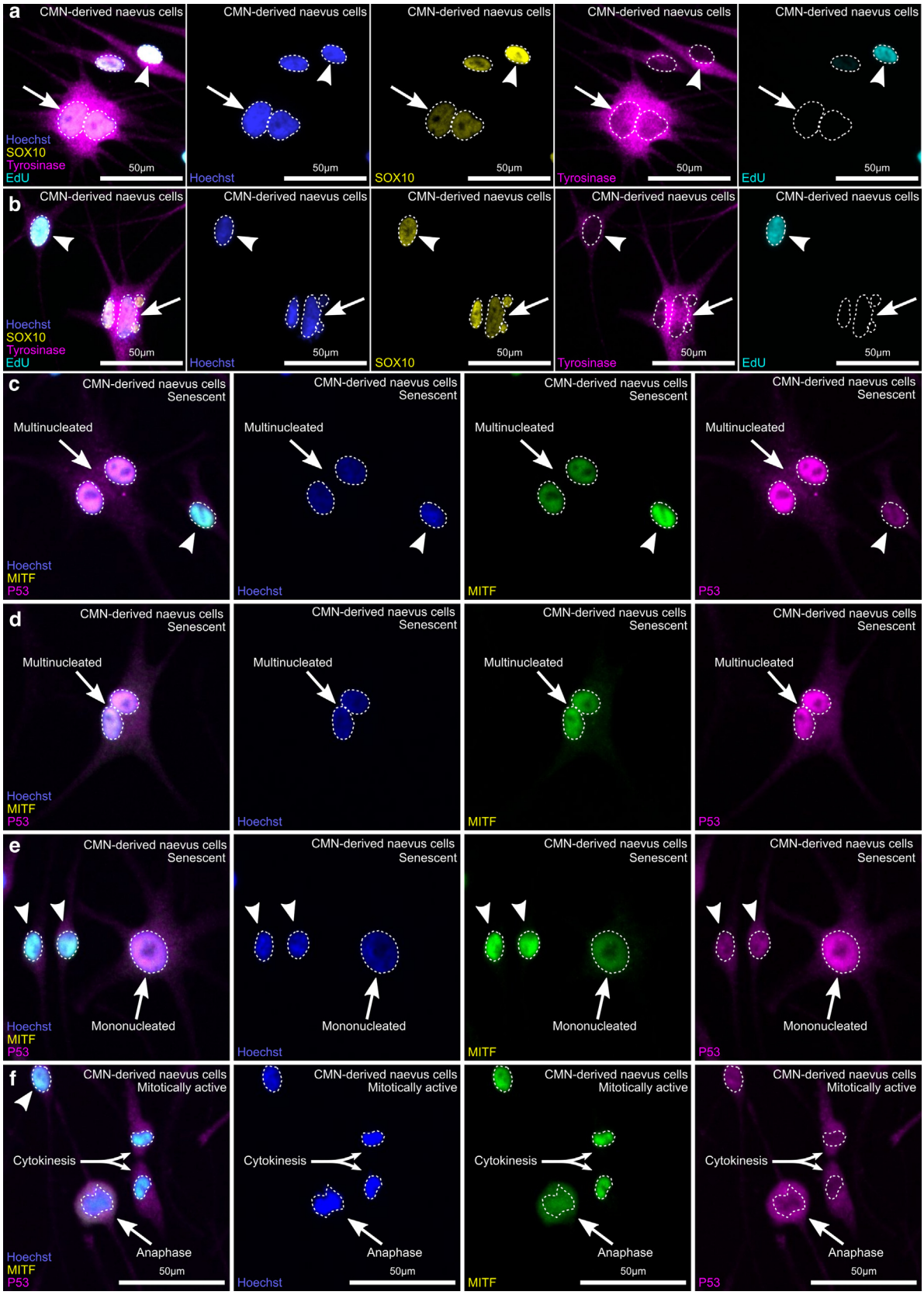

Supplementary Figure S5. Senescence in large and multinucleated nevus cells. Nevus cells (*NRAS c.181C>A (p.Q61K)*) with multiple nuclei containing (**a**) 2 nuclei or (**b**) fragmented nuclear compartments. (**c**–**e**) Nevus cells with multiple nuclei have elevated p53 expression (arrows). Cells with single nuclei are marked with arrow heads. (**f**) Cells with morphologies/Hoechst staining indicative of anaphase and cytokinesis have low p53 expression. Bars = 50 μm. CMN, congenital melanocytic nevus.

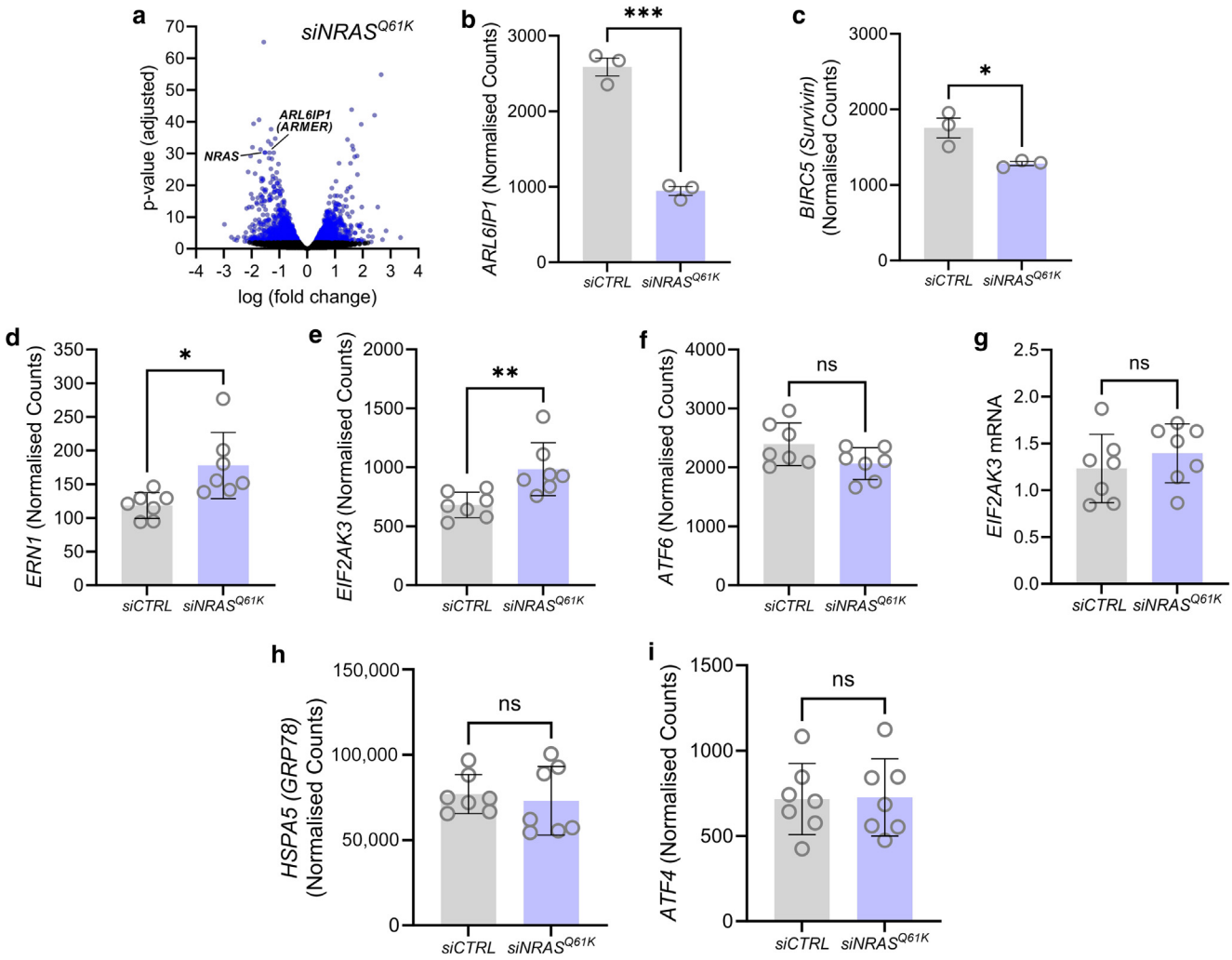

Supplementary Figure S6. Genes of interest in HCT116 dataset and endoplasmic reticulum stress–associated genes in nevus cell RNAseq dataset. (**a**–**c**) RNAseq expression data after 48-hour treatment of HCT116 cells (c.181C>A, NRASQ61K) with *siNRAS*^{Q61K}. (**a**) Volcano plot showing comparable decrease of *ARL6IP1* (ARMER) and *NRAS* expressions. (**b**) Decrease of *ARL6IP1* expression after treatment with *siNRAS*^{Q61K}. (**c**) Decrease of survivin (*BIRC5*) expression after treatment with *siNRAS*^{Q61K}. (**d**–**f**) RNAseq expression data of the 3 primary ER stress regulators (**d**) *ERN1* (*IRE1*), (**e**) *EIF2AK3* (*PERK*), (**f**) *ATF6*, (**h**) HSPA5, and (**i**) ATF4 after 48-hour treatment of nevus cells with *siNRAS*^{Q61K}. (**g**) qPCR validation of *EIF2AK3* result on RNAseq did not return a statistically significant difference. n = 7. Bars = mean, and error bars = SD, with 2-tailed unpaired *t*-test. ER, endoplasmic reticulum; ns, not significant; RNAseq, RNA sequencing; siCTRL, control-targeted small interfering RNA.

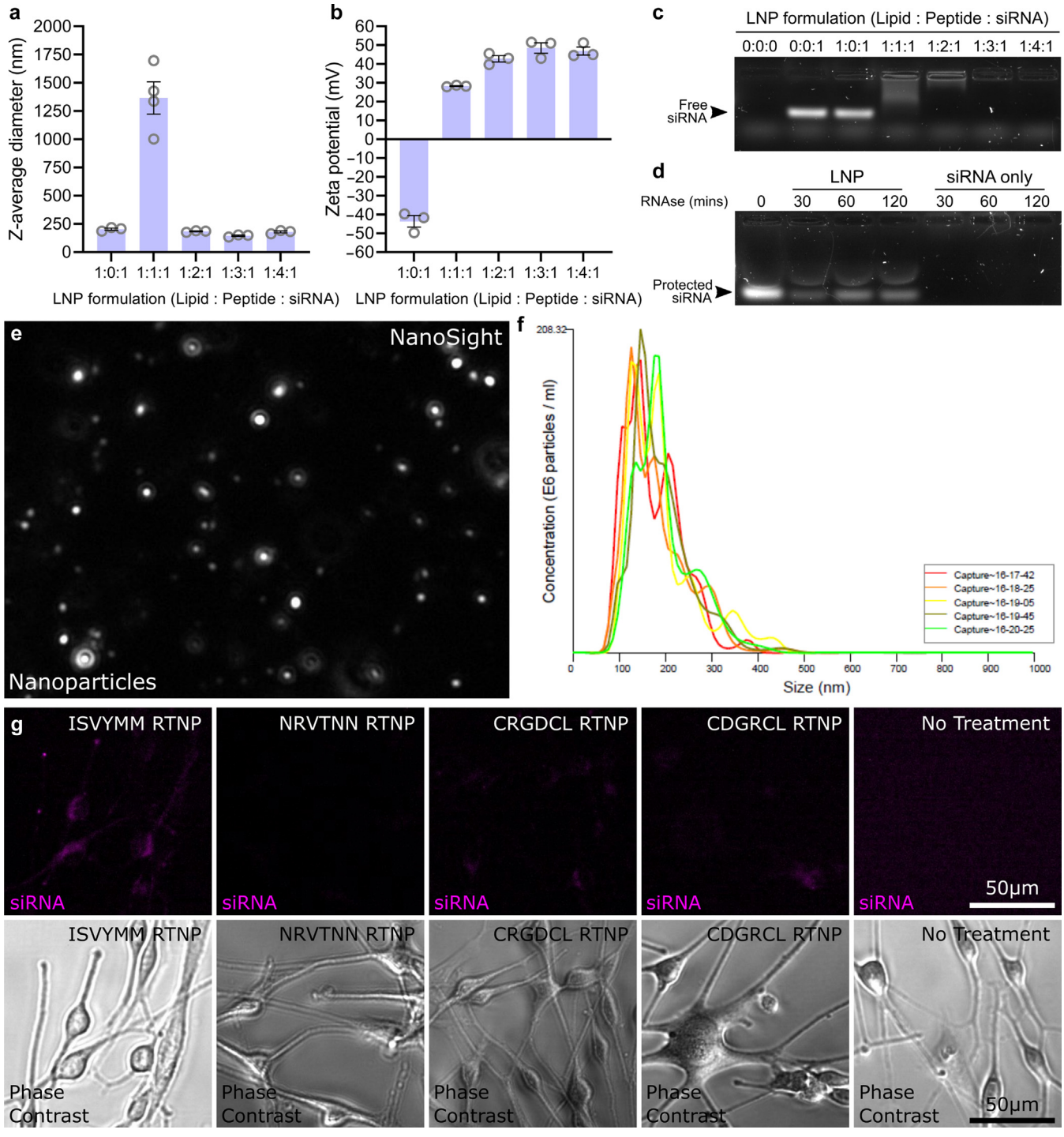

Supplementary Figure S7. Lipid nanoparticles. The (**a**) size (Zeta-average diameter), (**b**) charge (Zeta-potential), and (**c**) siRNA encapsulation of lipid nanoparticles formulated at different ratios were assessed. (**d**) Formulation of lipid nanoparticles at 1:4:1 (lipid:peptide:siRNA) ratios protected siRNA from RNases better than siRNA alone. (**e**) Visualization and (**f**) particle size distribution of RTNPs calculated with NanoSight instrument (Malvern). (**g**) Delivery of siRNA-cy5 to nevus cells with RTNPs formulated using different peptides (KKKKKKKKKKKKKKKKGACXXXXXXCG) with the targeting motif (XXXXXX): ISVYMM (reported to bind to KIT), NRVTNN (predicted to bind to KIT), CRGDCL (reported to bind to α5β1, αvβ5, and αvβ3 integrin), and CDGRCL (no known target). Bar = 50 μm. LNP, lipid nanoparticle; RTNP, receptor-targeted nanoparticle; siRNA, small interfering RNA.

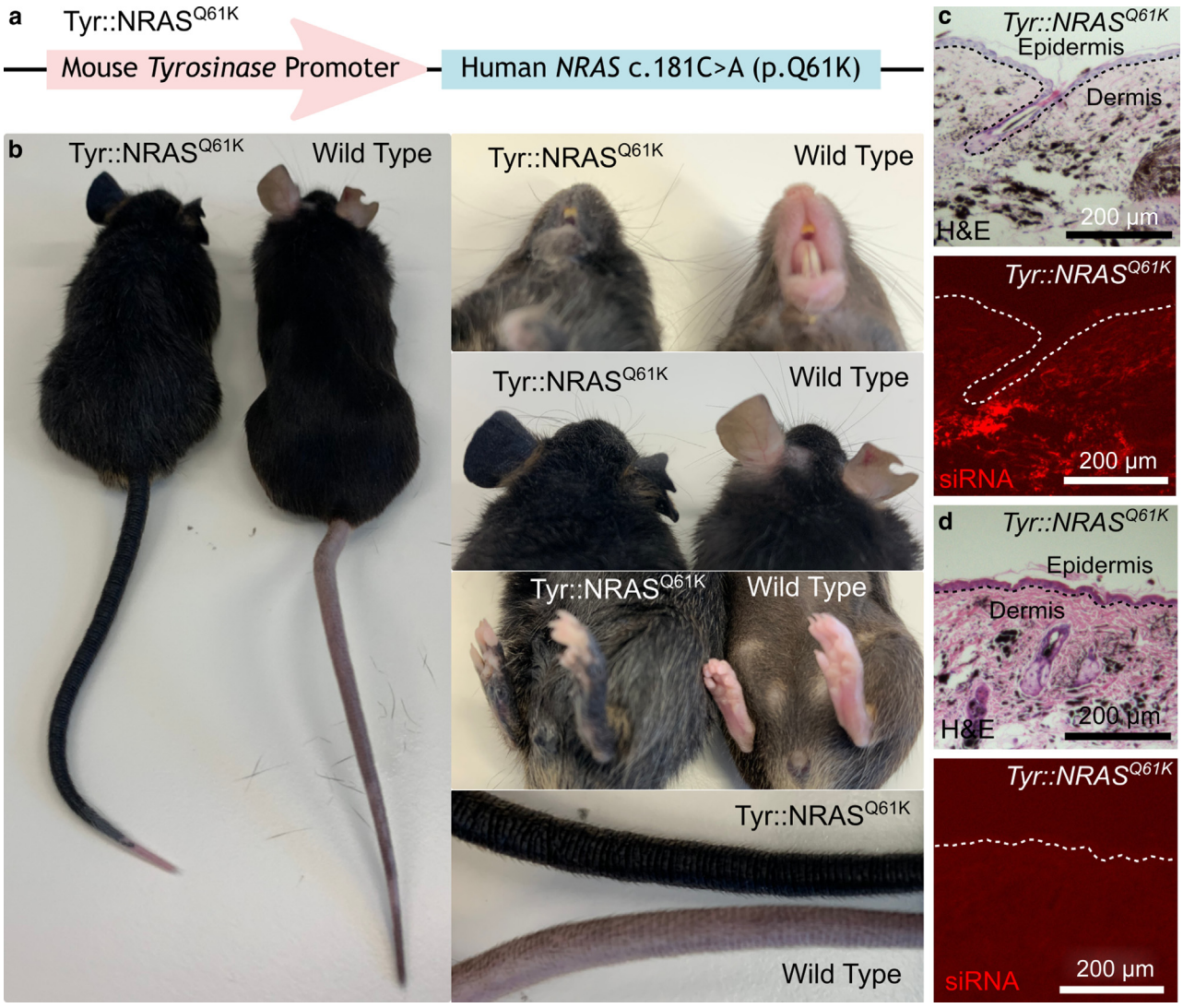

Supplementary Figure S8. Intradermal delivery of *siRNA* in mouse model of CMN. (**a**) Tyr::NRASQ61K mice (Tg(Tyr-NRAS*Q61K)1Bee in which expression of the human disease–causing variant *NRAS c.181C>A,p.(Q61K)* is driven by the endogenous mouse tyrosinase promoter. (**b**) Mice heterozygous for the transgene show widespread skin hyperpigmentation with accumulation of melanin-producing cells within the dermis, recapitulating the human phenotype of CMN to a large degree. (**c, d**) Biopsies of skin taken 1 hour after a single intradermal injection of (**c**) a fluorescent siRNA-Cy5 within lipid nanoparticles or (**d**) lipid nanoparticles only. CMN, congenital melanocytic nevus; siRNA, small interfering RNA.

Supplementary Table S1. Gene Expression Assays

Species	Gene	Type	Code/Forward	Reverse
Human	*NRAS (WT)*	Primers	CATACTGGATACAGCTGGAC	TTGATGGCAAATACACAGAGGA
Human	*NRAS (c.181C>A; p.(Q61K)*	Primers	CATACTGGATACAGCTGGAA	TTGATGGCAAATACACAGAGGA
Human	*GAPDH*	Primers	CAATGACCCCTTCATTGACC	AATTTGCCATGGGTGGAAT
Human	*ARL6IP1*	Taqman	Thermo Fisher Scientific, Hs00760013_s1	NA
Human	*ERN1*	Taqman	Thermo Fisher Scientific, Hs00980095_m1	NA
Human	*BIRC5*	Taqman	Thermo Fisher Scientific, Hs04194392_s1	NA
Human	*GAPDH*	Taqman	Thermo Fisher Scientific, Hs02786624_g1	NA
Mouse	*Nras*	Primers	GGACAGTTGACACAAAGCAAGCC	TGGCGTATCTCCCTTACCAGTG
Mouse	*Gapdh*	Primers	CATCACTGCCACCCAGAAGACTG	ATGCCAGTGAGCTTCCCGTTCAG
Mouse	*Arl6ip1*	Taqman	Thermo Fisher Scientific, Mm01274634_m1	NA
Mouse	*Gapdh*	Taqman	Thermo Fisher Scientific, Mm99999915_g1	NA

Abbreviation: NA, not available.

Supplementary Table S2. Formulation of Nevus Cell Media

Reagent	Vendor	Code	Formulation
Ham F-10 nutrient mix	Thermo Fisher Scientific	11550043	Basal medium
Fibroblasts GF basic	PeproTech	100-18B	2.5 ng/ml
Endothelin-1	Bachem	H-6995	10 ng/ml
3-isobutyl-1-methylxanthine	Sigma-Aldrich	I5879	31.5 μM
Cholera toxin	Sigma-Aldrich	C8052	0.33 nM
Phorbol 12-myristate 13-acetate	Sigma-Aldrich	P8139	5 nM
L-glutamine	Thermo Fisher Scientific	25030024	1x
Fetal bovine serum	Gibco	10270106	5% of total volume
Stem cell factor	Peprotech	300-07	20 ng/ml
Penicillin–streptomycin	Gibco	15070063	1×
Amphotericin B	Sigma-Aldrich	A2942	1×

Supplementary Table S3. Antibodies Used for Immunocytochemistry

Target	Species	Type	Code	Dilution	Blocking
Tyrosinase	Rabbit	IgG	AB170905	1:100	PBS, 10%FBS, 0.01% Triton X-100
MITF	Mouse	IgG1	AB3201	1:100	PBS, 10%FBS, 0.01% Triton X-100
Nestin	Rabbit	IgG	AB105389	1:100	PBS, 10%FBS, 0.01% Triton X-100
SOX10	Mouse	IgG	SC-365692	1:100	PBS, 10%FBS, 0.01% Triton X-100
DCT	Rabbit	IgG	AB74073	1:200	PBS, 10%FBS, 0.01% Triton X-100
CDKN2A	Mouse	IgG2a	SC-56330	1:200	PBS, 10%FBS, 0.01% Triton X-100
p53	Rabbit	IgG	CST-9282	1:100	PBS, 10%FBS, 0.01% Triton X-100
ARL6IP1	Rabbit	IgG	GTX85516	1:500	PBS, 10%FBS, 0.01% Triton X-100
RPN1	Goat	IgG	SC-12164	1:100	PBS, 10%FBS, 0.01% Triton X-100
Rabbit IgG AF594	Donkey	IgG	A21207	1:500	PBS, 10%FBS, 0.01% Triton X-100
Mouse IgG AF647	Donkey	IgG	A32787	1:500	PBS, 10%FBS, 0.01% Triton X-100

Abbreviation: FBS, fetal bovine serum.

Supplementary Table S4. Walked Design of Candidate siRNAs for Selective Silencing of *NRAS* c.181A>C

siRNA	Sense (+TT Overhang)	Antisense (+TT Overhang)	mRNA Complementarity
siRNA1	AUACUGGAUACAGCUGGAATT	UUCCAGCUGUAUCCAGUAUTT	*NRAS* c.163-181
siRNA2	UACUGGAUACAGCUGGAAATT	UUUCCAGCUGUAUCCAGUATT	*NRAS* c.164-182
siRNA3	ACUGGAUACAGCUGGAAAATT	UUUUCCAGCUGUAUCCAGUTT	*NRAS* c.165-183
siRNA4	CUGGAUACAGCUGGAAAAGTT	CUUUUCCAGCUGUAUCCAGTT	*NRAS* c.166-184
siRNA5	UGGAUACAGCUGGAAAAGATT	UCUUUUCCAGCUGUAUCCATT	*NRAS* c.167-185
siRNA6	GGAUACAGCUGGAAAAGAATT	UUCUUUUCCAGCUGUAUCCTT	*NRAS* c.168-186
siRNA7	GAUACAGCUGGAAAAGAAGTT	CUUCUUUUCCAGCUGUAUCTT	*NRAS* c.169-187
siRNA8	AUACAGCUGGAAAAGAAGATT	UCUUCUUUUCCAGCUGUAUTT	*NRAS* c.170-188
siRNA9	UACAGCUGGAAAAGAAGAGTT	CUCUUCUUUUCCAGCUGUATT	*NRAS* c.171-189
siRNA10	ACAGCUGGAAAAGAAGAGUTT	ACUCUUCUUUUCCAGCUGUTT	*NRAS* c.172-190
siRNA11	CAGCUGGAAAAGAAGAGUATT	UACUCUUCUUUUCCAGCUGTT	*NRAS* c.173-191
siRNA12	AGCUGGAAAAGAAGAGUACTT	GUACUCUUCUUUUCCAGCUTT	*NRAS* c.174-192
siRNA13	GCUGGAAAAGAAGAGUACATT	UGUACUCUUCUUUUCCAGCTT	*NRAS* c.175-193
siRNA14	CUGGAAAAGAAGAGUACAGTT	CUGUACUCUUCUUUUCCAGTT	*NRAS* c.176-194
siRNA15	UGGAAAAGAAGAGUACAGUTT	ACUGUACUCUUCUUUUCCATT	*NRAS* c.177-195
siRNA16	GGAAAAGAAGAGUACAGUGTT	CACUGUACUCUUCUUUUCCTT	*NRAS* c.178-196
siRNA17	GAAAAGAAGAGUACAGUGCTT	GCACUGUACUCUUCUUUUCTT	*NRAS* c.179-197
siRNA18	AAAAGAAGAGUACAGUGCCTT	GGCACUGUACUCUUCUUUUTT	*NRAS* c.180-198
siRNA19	AAAGAAGAGUACAGUGCCATT	UGGCACUGUACUCUUCUUUTT	*NRAS* c.181-199

Abbreviation: siRNA, small interfering RNA.

Supplementary Table S5. Antibodies Used for Western Blotting

Target	Species	Type	Code	Dilution	Blocking
Total ERK	Mouse	IgG	CST-9107	1:1000	TBS, 5% fish gelatin, 0.1% Tween-20
pERK	Rabbit	IgG	CST-4377	1:1000	TBS, 5% fish gelatin, 0.1% Tween-20
NRAS	Mouse	IgG	SC-31	1:100	TBS, 3% BSA, 0.1% Tween-20
Vinculin	Mouse	IgG1	MA5-11890	1:5000	TBS, 3% BSA, 0.1% Tween-20
Mouse IgG HRP	Goat	IgG	P-0447	1:5000	TBS, 0.1% Tween-20
Rabbit IgG HRP	Goat	IgG	P-0448	1:5000	TBS, 0.1% Tween-20
Mouse IgG IRDye 680RD	Goat	IgG	926-68071	1:7000	TBS, 0.1% Tween-20
Rabbit IgG IRDye 800CW	Goat	IgG	926-32210	1:10,000	TBS, 0.1% Tween-20

Abbreviations: ERK, extracellular signal–regulated kinase; HRP, horseradish peroxidase; pERK, phosphorylated extracellular signal–regulated kinase; TBS, Tris buffered saline.